Supernova Remnants at High Energy

Stephen P. Reynolds

Physics Department, North Carolina State University, Raleigh, North Carolina 27695;
email: stephen_reynolds@ncsu.edu

Annu. Rev. Astron. Astrophys. 2008. 46:89–126

First published online as a Review in Advance on May 19, 2008

The *Annual Review of Astronomy and Astrophysics* is online at astro.annualreviews.org

This article's doi:
10.1146/annurev.astro.46.060407.145237

0066-4146/08/0922-0089$20.00

Key Words

cosmic rays, gamma-ray sources, shock acceleration, X-ray sources

Abstract

Many shell supernova remnants are now known to radiate synchrotron X-rays. Several objects have also been detected in TeV gamma rays. Nonthermal X-rays and gamma rays can be produced in shell remnants by extremely energetic ions and electrons due to decay of π^0 mesons produced in inelastic collisions between ions and thermal gas, or by electron synchrotron, bremsstrahlung, or inverse-Compton radiation. Thus observations at X-ray and gamma-ray wavelengths constrain the process of particle acceleration to high energies in the shock waves of supernova remnants. This review examines the relevant characteristics of Type Ia and core-collapse supernovae, the dynamics of their evolution through the Sedov blast-wave phase, the basic physics of diffusive shock acceleration, and the physics of the relevant radiative processes. It also reviews the current status of observations of shell remnants from X-rays to TeV gamma rays, and summarizes what we can learn about particle acceleration.

1. INTRODUCTION

SNR: supernova remnant

CSM: circumstellar medium (modified by SNR progenitor's winds)

ISM: interstellar medium (unmodified by SNR progenitor)

Shell supernova remnants (SNRs) illustrate the interaction of several solar masses of processed stellar ejecta, carrying of order 10^{51} erg of kinetic energy, with surrounding circumstellar (modified by the progenitor) or interstellar (unmodified) medium (CSM or ISM). The resulting strong shock waves have initial speeds of several thousand kilometers per second, gradually decelerating over tens of thousands of years. They heat ambient gas and ejecta to X-ray-emitting temperatures until speeds fall below a few hundred kilometers per second. Recent theory and observation have revealed that these shocks put some fraction of their energy into accelerated, nonthermal particles and magnetic field. The fractions can be large, with substantial impact both on the remnant dynamics and on the Galactic population of cosmic-ray particles. Electrons with energies of 100 TeV and above are inferred to be present in SNRs. I review the observations of nonthermal X-rays and gamma-rays from SNRs on which these inferences are based, and the background of SNR dynamics, strong-shock physics, and radiative processes required to interpret them. I do not discuss phenomena associated with any neutron stars or pulsars left behind by the explosions, including pulsar wind nebulae (PWNe).

2. A BRIEF HISTORY

The first remnants of supernovae to be identified were optical nebulosities associated with historical supernovae, but with the advent of radio interferometry in the early 1950s, it became clear that the Galaxy held a substantial population of extended objects with nonthermal (power-law, flux $S_\nu \propto \nu^\alpha$ with $\alpha \sim -0.5$) radio spectra. Shklovskii (1953) first proposed that the emission process was synchrotron radiation, and that these sources should be identified as remnants of unseen supernovae. Radio emission is still the most common identifier of remnants; the bulk of the 250 or so Galactic SNRs are identified as extended radio sources with steep spectra (Green 2006). Shklovskii's suggestion meant that from the beginning, SNRs were inferred to be sources of nonthermal, power-law populations of relativistic electrons (or positrons), emitting synchrotron radiation. Standard synchrotron physics (e.g., Pacholczyk 1970) relates the power-law electron and photon distributions: a distribution $N(E) = KE^{-s}$ electrons cm^{-3} erg^{-1} produces a power-law photon distribution with $\alpha = (1 - s)/2$. Observed values of $\alpha \sim -0.5$ imply $s \sim 2$, close to the 2.7 or so observed in cosmic-ray particles of a few GeV and up arriving at Earth (e.g., Gaisser 1990). Furthermore, in a magnetic field B G, an electron of energy E radiates its peak power at a frequency $\nu = 1.82 \times 10^{18} E^2 B$ Hz, so that $E = 14.7(\nu_{\rm GHz}/B_{\mu \rm G})^{1/2}$ GeV. It was thus clear, once Shklovskii's suggestion was accepted, that shell SNRs contained electrons with energies in the GeV range, millions of times higher than the energies expected from thermalization behind a shock of speed 10^3 km s^{-1}, as inferred in historical remnants.

Particles of such energies were already known in astrophysics, as cosmic rays. Above about 1 GeV, cosmic rays are primarily from outside the heliosphere. They are mostly protons, but ions of most of the elements in the periodic table are represented, as well as electrons and a few positrons and antiprotons (e.g., Gaisser 1990). The all-particle spectrum can be well described by power-law distributions: $\propto E^{-2.7}$ up to a slight steepening near 3000 TeV known as the knee, with a slope of about 3.0–3.2 continuing to above 10^{19} eV. It is normally assumed that a single mechanism is responsible for producing Galactic cosmic rays up to the knee, whereas both Galactic and extragalactic models have been proposed for higher energies. Radioactive secondaries such as ^{10}Be in the cosmic rays allow a mean age to be inferred for particles of energies of a few GeV per nucleon of about 20 million years (Gaisser 1990). Requiring that the Galactic volume of cosmic rays be replenished on that timescale gives an energetic requirement of about 10^{48} erg year^{-1} for ions (about 2% of this for electrons).

Fermi (1949) had proposed a statistical, diffusive cosmic-ray acceleration process in which collisions through magnetic mirroring between charged particles and interstellar clouds could result in the production of a suprathermal, power-law population. This idea was proposed as the mechanism for supernovae and remnants as well, but various problems accompanied its application there. Fermi's diffusive acceleration produced energy gains of second order in the ratio of cloud velocity u to particle speed v, because to first order approaching and receding collisions produced cancelling effects. Acceleration rates were thus relatively slow, and the resulting spectrum depended on a free parameter, the escape timescale. It was realized roughly simultaneously by several researchers (Axford, Leer & Skadron 1977; Krymsky 1977; Bell 1978; Blandford & Ostriker 1978) that in a strong shock wave, a reference frame existed (not the shock frame) in which preshock and postshock fluids converged, so that a particle scattered from scattering centers embedded in these fluids would experience only approaching collisions, allowing energy gains first-order in u/v and much more rapid acceleration, with a resulting spectrum depending only on the shock compression ratio (for energetically unimportant test particles). This proposal, diffusive shock acceleration (DSA) or first-order Fermi acceleration, was rapidly accepted as the explanation for the radio-emitting electrons inferred in SNRs. Because cosmic-ray energies range to 10^{19} eV, not just to the $\sim 10^{10}$ eV or so required by radio observations, it was natural to suggest that SNRs could produce such energies as well.

DSA: diffusive shock acceleration

Reynolds & Chevalier (1981) first proposed that DSA could accelerate electrons to synchrotron-X-ray-emitting energies in the shell of the historical remnant of SN 1006 AD (**Figure 1**) to explain that remnant's almost featureless X-ray spectrum (Becker et al. 1980). Their model, however, assumed that radiative losses began to take effect only after acceleration to very high energies. Lagage & Cesarsky (1983) calculated the maximum energies expected for DSA in evolving shell supernova remnants, finding energies of at most 10^{14} eV, not even as high as the knee. Later X-ray observations of SN 1006 (Galas, Venkatesan & Garmire 1982) showed clear O lines below 1 keV. However, the spatially resolved X-ray spectroscopy possible with the Japanese *ASCA* satellite in 1993 (Koyama et al. 1995) showed that the X-ray spectrum of SN 1006 varied strongly with position: the bright limbs showed completely featureless spectra well described with a power-law, whereas the interior showed a typical thermal spectrum of a young supernova remnant. Updates of the Reynolds & Chevalier model (Ammosov et al. 1994, Reynolds 1998) showed that careful accounting for acceleration and energy-loss rates gave an integrated electron energy distribution whose synchrotron emission curved broadly around a rolloff photon energy in the

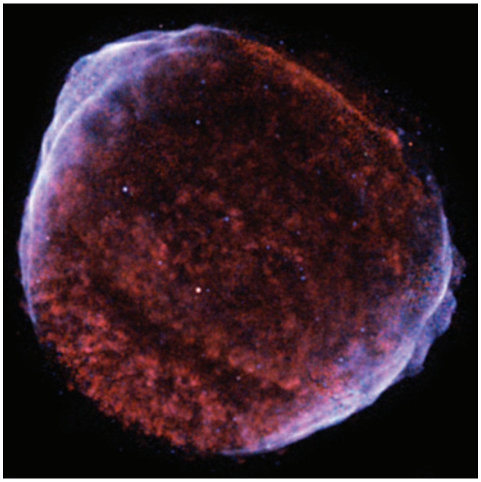

Figure 1

Chandra X-ray image of the remnant of the supernova of 1006 AD. Red, 0.5–0.9 keV; cyan, 0.91–1.34 keV; blue, 1.3–3.0 keV. Hard X-rays (synchrotron) are confined to narrow limbs in thin filaments. Soft X-rays are largely thermal. (Image courtesy of NASA/CXC.)

IC: inverse-Compton

ICCMB: inverse-Compton from cosmic microwave background photons

appropriate range. Reynolds (1998) showed that the limb spectrum of SN 1006 could be well fit by such a model, with a rolloff energy of order 100 TeV. These results for SN 1006 were the first demonstration of the presence of particles with such energies in the putative sources of Galactic cosmic rays.

Two more synchrotron-dominated shell SNRs were discovered in the late 1990s: RX J1713.7-3946 (Koyama et al. 1997, Slane et al. 1999) (also known as G347.3-0.5) and G266.2-1.2 (Vela Jr.) (Aschenbach 1998, Slane et al. 2001). Synchrotron components were inferred to be present in thin filaments at the edges of historical remnants Tycho (Hwang et al. 2002, Warren et al. 2005), Kepler (Cassam-Chenaï et al. 2004a), and Cas A (Bleeker et al. 2001, Gotthelf et al. 2001), and a synchrotron continuum added to thermal emission satisfactorily explained apparently very weak lines in RCW 86 (Rho et al. 2002, Vink et al. 2006). A simple exponential cutoff in the electron spectrum gave a similar result to the elaborate models of Reynolds (1998), and has now been used by many researchers to explain the spectra of these objects. Synchrotron X-ray emission from shell SNRs is now widely accepted as a possible contributor to observed spectra, and is used as a diagnostic of physical conditions.

If shell SNRs were to produce Galactic cosmic rays even up to the knee energy, several other processes should produce high-energy photons. Synchrotron emission would show the highest-energy electrons; but lower energy nonthermal electrons should radiate bremsstrahlung with characteristic photon energies of about one-third the electron energy, resulting in a continuum extending from keV to TeV energies. In addition, such highly energetic electrons could upscatter any photon fields present to much higher energies by the inverse-Compton (IC) process; in particular, upscattering of cosmic microwave background radiation (ICCMB) would produce TeV photons from 10–100 TeV electrons, so it should be a firm prediction of the synchrotron hypothesis (Mastichiadis 1996, Pohl 1996). Its measurement would give directly the relativistic-electron density without requiring knowledge of the magnetic field, which could then be deduced from observed synchrotron fluxes. Finally, the energetically dominant hadronic component presumed also to be accelerated by the same shock waves should give rise to inelastic scattering of cosmic-ray ions on thermal protons and production of pions. Charged pions would ultimately contribute a negligible number of additional electrons or positrons to the accelerated-electron pool, but π^0 mesons would decay to gamma rays, producing a spectral component turning on around 70 MeV and continuing with the same shape as the primary ion spectrum (Drury, Aharonian & Völk 1994). Predictions for the spectra produced by these four processes were made by several groups (Sturner et al. 1997; Gaisser, Protheroe & Stanev 1998; Baring et al. 1999).

One motivation for this outburst of theoretical work was the publication of a list of possible associations between known supernova remnants and unidentified Galactic-plane gamma-ray sources observed with the EGRET instrument on the *Compton Gamma Ray Observatory* satellite (Esposito et al. 1996), at energies from 100 MeV to about 20 GeV. Spectra of the candidates presented by Esposito et al. (1996) were featureless power-laws of photon index Γ about 2 ($F_E \propto E^{-\Gamma}$ photons cm^{-2} s^{-1} MeV^{-1}), providing relatively little information. Although earlier gamma-ray satellites such as SAS-2 and COS-B had imaged the gamma-ray sky with angular resolutions of a few degrees and located several discrete sources, predictions for gamma-ray emission from shell SNRs began in earnest under this EGRET stimulus.

TeV photon emission has now been reported from G347.3-0.5 (Enomoto et al. 2002), with the CANGAROO air-Čerenkov telescope in Australia, and from G266.2-1.2 (Aharonian et al. 2007a), with the High Energy Stereoscopic System (H.E.S.S.) collaboration in Namibia. The H.E.S.S. collaboration has continued to report detections and upper limits from other supernova remnants, though many of its sources are probably gamma-ray pulsars or PWNe. These results have been modeled with elaborate shock-acceleration physics (e.g., Berezhko & Völk 2006). Observation of the π^0 bump around 70 MeV that would give the first direct evidence for the presence of cosmic-ray ions in SNRs has not yet occurred; the relevant energy range (10 MeV–1 GeV) has not been accessible since the demise of EGRET. The GLAST telescope should improve the situation dramatically, and the SNR community holds high hopes for the direct inference of cosmic-ray ions from shell SNRs.

CC: core-collapse

Understanding and interpreting high-energy radiation from SNRs involve overall SNR dynamics, shock-acceleration theory, and radiative processes. These subjects are briefly reviewed in turn, followed by a summary of current observations of SNRs at high energy.

3. SUPERNOVA-REMNANT EVOLUTION

The past twenty years have seen impressive strides in our understanding of supernovae. The original simple classification of Type I (no H lines at maximum light) and Type II (with H) has been elaborated, most importantly with the discovery that some Type Is, now called Ib, lack a spectral feature of Si II (6150 Å), and look much more like Type IIs at later times (though still without H). Type I is now subdivided into Ia, Ib, and Ic, with Ib and Ic associated with massive-star populations, and Ic lacking He as well as H lines. The nuclear burning of a carbon-oxygen white dwarf to iron-peak elements would produce about 10^{51} erg; this remains the best explanation for Type Ia (thermonuclear) supernovae. All others appear to be the explosions of massive stars powered by gravitation (core-collapse, CC). Stars above about 8 $M_\odot$ can explode as red supergiants (RSGs), giving rise to a plateau in the light curve (Type IIP), as supergiants with lower-mass H envelopes undergoing a more linear decline after maximum light (Type IIL), or as cores having ejected their H envelopes (Type Ib) or both H and He envelopes (Type Ic), the latter presumably in an earlier Wolf-Rayet phase. Some CC events show spectra with narrow emission lines (Type IIn). A CC explosion is powered by the $\sim$0.3% of the gravitational binding energy of a 1.4-$M_\odot$ neutron star that is not carried away by neutrinos, which is also about 10^{51} erg. So once the composition of the ejected material is no longer evident, the gross evolution of remnants of thermonuclear and CC explosions is similar.

The initial density and velocity structure of the progenitor star shortly after the shock wave breaks out is important for subsequent evolution. For spherically symmetric CC explosions, Matzner & McKee (1999) show that once freely expanding, the ejecta form a relatively uniform-density core surrounded by an envelope with steeply dropping density, fairly well described by a power-law, $\rho \propto r^{-n}$ with $n \sim 10 - 12$. The explosion of a white dwarf produces an ejecta profile that is fairly well described by a power-law of index 7 (Colgate & McKee 1969); however, an exponential gives a better match to hydrodynamic simulations (Dwarkadas & Chevalier 1998).

CC progenitors are expected to modify their surroundings by episodes of mass loss, at least a fast wind during their main-sequence lifetimes and a slower, dense wind in RSG phases. These winds would leave CSM with a density profile $\rho \propto r^{-s}$ with $s = 2$, into which the supernova would occur. Evidence for such CSM is amply provided by prompt X-ray and radio emission from CC SNe. Type Ia events do not show such signatures, placing strong upper limits on the density of any CSM. (The use of s for the ambient-medium density index is standard, unfortunately; in this review its use for this purpose is restricted to this section. Elsewhere s is used for the power-law index of particle energy distributions.)

Both ejecta and CSM may be quite inhomogeneous. Inhomogeneities on small scales should not produce large departures from results assuming spherical symmetry, but major inhomogeneities, such as jet-driven supernovae or CSM in equatorial disks, would not be well described by these simple results and are beyond the scope of this review. The roughly spherical shape of most young SNRs indicates that such major departures do not typically dominate the gross evolution.

The Rankine-Hugoniot relations conserving mass, momentum, and energy across a planar, adiabiatic shock front give standard results for post-shock temperatures and pressures (if magnetic pressure is negligible). We assume the shock is a discontinuity in flow velocity that is otherwise constant on either side of the shock at values u_1 and u_2 up- and downstream. Let the compression ratio $r_{\rm comp} \equiv \rho_2/\rho_1$. The shock (sonic) Mach number is given by $\mathcal{M}^2 \equiv \rho_1 u_1^2/\gamma p_1$, where γ is the ratio of specific heats. Then (e.g., Spitzer 1978)

$$\frac{u_2}{u_1} \equiv \frac{1}{r_{\rm comp}} = \frac{\gamma - 1}{\gamma + 1} + \frac{2}{\gamma + 1}\frac{1}{\mathcal{M}^2}, \tag{1}$$

$$\frac{p_2}{p_1} = \frac{2\gamma}{\gamma + 1}\mathcal{M}^2 - \frac{\gamma - 1}{\gamma + 1}, \tag{2}$$

where p is the pressure. For the common and important case of $\gamma = 5/3$ and $\mathcal{M}^2 \gg 1$, we have the well-known results

$$r_{\rm comp} = \frac{\rho_2}{\rho_1} = \frac{\gamma + 1}{\gamma - 1} = 4, \tag{3}$$

$$p_2 = \frac{2\rho_1 u_1^2}{\gamma + 1} = \frac{3}{4}\mu_1 m_p n_1 u_1^2, \tag{4}$$

$$kT_2 = \frac{3}{16}\mu_2 m_p u_1^2, \tag{5}$$

where μ is the mean mass per particle ($\mu \cong 0.6$ for fully ionized gas of cosmic composition, probably the case downstream; upstream, μ_1 may be 1.4, the value for neutral gas of cosmic composition), and n_1 is the upstream particle number density.

These relations hold in the case that energy loss owing to radiation (or other causes) is negligible. However, efficient shock acceleration, as discussed in the next section, can lead to significant energy loss by escaping nonthermal particles. In addition, an energetically significant relativistic-particle population will lower the mean adiabatic index from 5/3 toward its fully relativistic value of 4/3. Both effects will increase shock compression ratios at the least, and can affect the overall shock evolution. Typical calculations (e.g., Ellison & Cassam-Chenaï 2005) demonstrate some of these effects: the separations between forward shock, contact discontinuity, and reverse shock (see below) can be markedly reduced. A change in the adiabatic index will not alter the time dependence of shock radius found for the self-similar solutions below, but major energy loss due to escaping particles could conceivably change expansion rates. Evidence from observed expansion of remnants of known age, beyond the scope of the present review, does not appear to show large departures from the adiabatic rates, though detailed morphological effects resulting from higher compression ratios have been claimed (e.g., Warren et al. 2005; Völk, Berezhko, & Ksenofontov 2007).

Although supernovae eject a mass $M_{\rm ej}$ of material with a range of velocities, a characteristic initial explosion velocity $(2E_{\rm SN}/M_{\rm ej})^{1/2}$ is of order 10^4 km s^{-1} for a Type Ia and 5000 km s^{-1} for a CC event—far higher than the expected sound speeds c_s of order 1–10 km s^{-1} in the surrounding ISM or CSM. Thus an extremely high Mach-number ($\mathcal{M} \gtrsim 10^3$) blast wave is formed. Behind it, the ejecta initially expand almost freely, and rapidly cool adiabatically to very low temperatures. The ejecta rapidly sort themselves into a Hubble law velocity profile $v \propto r$. Whether a SN blast wave encounters modified CSM or relatively undisturbed interstellar medium, it takes only a few days for the shock to slow enough that interior ejecta are decelerated abruptly, and reheated, by an inward-facing reverse shock. We may call this the ejecta-driven phase. The reverse shock begins life very weak and radiative, but rapidly strengthens to velocity jumps of order 1000 km s^{-1}, producing X-ray-emitting temperatures in the ejecta. In spherical symmetry, the shock-heated ambient ISM or CSM is separated from the shock-heated ejecta by a contact discontinuity across which the pressure is constant; more realistically, one expects this surface to be Rayleigh-Taylor unstable once significant deceleration occurs, producing strong turbulence. The two-shock structure will persist until an amount of mass comparable to the ejected mass has been swept up, at which point all the ejecta will have been shocked and the evolution can be described by the Sedov self-similar solution for an adiabatic point explosion in a uniform medium of negligible pressure (Sedov 1959).

If the outer ejecta density profile is a sufficiently steep power-law, the two-shock structure also evolves self-similarly (Chevalier 1982, Nadyozhin 1985) and is called a self-similar driven wave (SSDW). The self-similarity, with constant ratios between the radii of the forward shock, reverse shock, and contact discontinuity, persists until the reverse shock reaches the inner ejecta where the density is close to constant. At that point, the reverse shock will accelerate toward the center and fairly rapidly shock the remaining ejecta. This is a reasonable approximation for CC events, but a power-law is not as good an approximation for Type Ia events. Dwarkadas & Chevalier (1998) presented numerical simulations for more realistic exponential density profiles for white-dwarf ejecta. The results differ substantially from the power-law case, as no self-similarity is possible.

The self-similar solutions give a simple scaling for the blast-wave radius R (Chevalier 1982):

$$R \propto t^{(n-3)/(n-s)}, \tag{6}$$

where we expect $n = 10$–12 and $s = 2$ for CC events. For a Type Ia event, we expect interaction with undisturbed ISM, $s = 0$; using the approximate value $n \sim 7$ for a white dwarf allows a similarity solution as well. For an $n = 7$ white-dwarf model, Equation 6 gives a radius varying as $R \propto t^m$, with $m = 4/7$ (for ISM) or $4/5$ (for a Type Ia progenitor with a white-dwarf wind). For a CC event with $n \sim 11$ and $s = 2$, we have $m = 8/9$. Proper-motion determinations of expansion have been made for several young remnants (Moffett, Goss & Reynolds 1993, and references therein), which seem to show m between these values and the 2/5 characterizing the later Sedov phase.

The two-shock phase of SNR evolution should last for hundreds to thousands of years, depending in particular on the structure of the surrounding material. In spherical symmetry, the reverse shock will eventually move inward to the remnant center and disappear, having shocked and reheated all the ejecta; however, in more realistic hydrodynamic simulations, various reverberations occur, prolonging the life of reverse shocks. In 1D analytic calculations and simulations, the transition to Sedov-Taylor evolution requires that several times the amount of the ejected mass have been swept up. **Figure 2** shows this transition, calculated with a 1D hydrodynamic simulation,

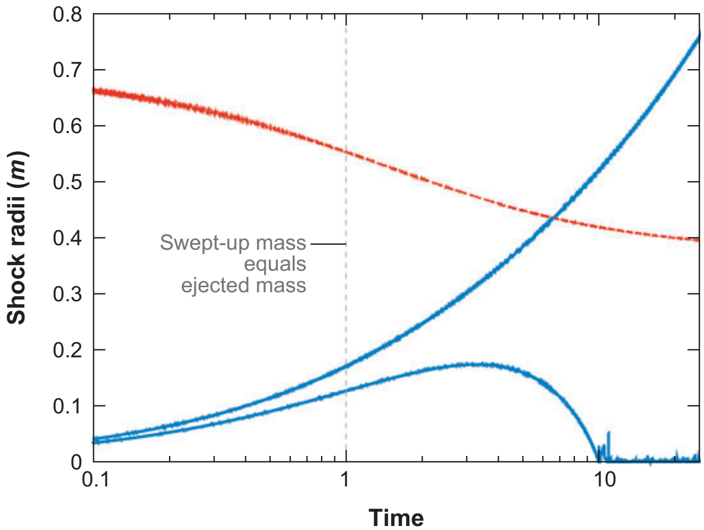

Figure 2

Forward and reverse shock radii (*blue lines*) and $m \equiv vt/R$ (*red line*), from a 1D hydrodynamic simulation. Note the gradual transition to the Sedov phase $m = 0.4$.

beginning with the harmonic-mean density profile used by Truelove & McKee (1999). The figure shows radii of the blast wave and reverse shock, as well as m.

However, eventually one expects that the dynamics will be well approximated as a Sedov blast wave. A characteristic value for the ejecta-driven to Sedov transition time, $t_{\rm ch}$, can be found from dimensional analysis assuming the only relevant parameters are ejected mass $M_{\rm ej}$, explosion energy E, and ambient density ρ_0 (Truelove & McKee 1999):

$$t_{\rm ch} = E^{-1/2} M_{\rm ej}^{5/6} \rho_0^{-1/3}, \tag{7}$$

This phase, lasting up to tens of thousands of years, is commonly called the Sedov phase. For a specific heat ratio of 5/3 (which will not be correct for cosmic-ray-dominated shocks; see below), the shock radius, velocity, and temperature obey

*Errata

$$R = 1.15(E/\rho_0)^{1/5} t^{2/5} = 0.31 E_{51}^{1/5} (\mu_1/1.4)^{-1/5} n_0^{-1/5} t_{\rm yr}^{2/5} \text{ pc}, \tag{8}$$

$$u = 0.4\, R_s/t = 123{,}000\ E_{51}^{1/5} (\mu_1/1.4)^{-1/5} n_0^{-1/5} t_{\rm yr}^{-3/5} \text{ km s}^{-1}, \tag{9}$$

$$kT = (3/16)\mu_2 m_p u^2 = 1.78 \times 10^4 (\mu_2/0.6) E_{51}^{2/5} (\mu_1/1.4)^{-2/5} n_0^{-2/5} t_{\rm yr}^{-6/5} \text{ keV}, \tag{10}$$

where μ is the mean mass per particle. Truelove & McKee (1999; see also Errata 2000) have carried out extensive analytic and numerical calculations in one dimension covering the ejecta-driven and Sedov phases.

The Sedov phase ends when the shock is slow enough that significant radiative cooling can take place and the adiabatic approximation breaks down. However, local regions of the blast wave may become radiative sooner where the ambient density is much higher than average, though the bulk evolution is still adiabatic. Once most of the shock is radiative, the interior may still remain hot enough to provide significant pressure (pressure-driven snowplow); if the interior is able to cool, the shell can continue to coast outward in the momentum-conserving phase.

For fully ionized, cosmic-abundance gas, and approximating the gas volume cooling function as $\Lambda(T) = 10^{-16} T^{-1}$ ergs cm^3 s^{-1}, Blondin et al. (1998) find at the transition to radiative evolution

$$t_{\rm tr} = 2.9 \times 10^4\ E_{51}^{4/17}\ n_0^{-9/17} \text{ year}, \tag{11}$$

$$R_{\rm tr} = 19\, E_{51}^{5/17}\ n_0^{-7/17} \text{ pc}, \tag{12}$$

$$M_{\rm tr} = 10^3\ E_{51}^{15/17}\ n_0^{-4/17}\ M_\odot, \tag{13}$$

where $M_{\rm tr}$ is the mass swept up by that time (assuming a uniform ambient medium). Blondin et al. (1998) find that in numerical simulations a cold, dense shell of gas forms fairly abruptly at $t \sim (1.5 - 1.9)t_{\rm tr}$ for ambient densities between 0.1 and 100 cm^{-3}. After about $(2-3)t_{\rm tr}$, the expansion settles down to a rate $m \sim 0.33$. The shock velocity at $2t_{\rm tr}$ is of order 100–300 km s^{-1}, and the hydrodynamic Mach number is of order 3–6. Such blast wave speeds are slow enough that particle acceleration is not likely to be important to the energies required for keV–TeV photon production. The results in the next section show that the most important phases for particle acceleration are pre-Sedov and through the transition into the Sedov phase.

4. PARTICLE ACCELERATION

As described above, radio emission from SNRs already indicates the presence of ultrarelativistic ($E \sim 10^4 m_e c^2$) electrons. These electrons could in principle simply be borrowed from the interstellar medium, compressed in the remnant shock wave. Two arguments summarized in Reynolds (1988a) suggest that this mechanism cannot explain radiation from young remnants with adiabatic shocks and compression ratios r_{comp} of order four. First, the spectrum is incorrect, compared to the diffuse Galactic synchrotron background. Second, many SNR shells have a radio brightness far too high to be explainable simply by compression of interstellar electrons and magnetic field; although the synchrotron emissivity should rise roughly as r_{comp}^3, observed emissivities exceed those in the ISM by up to four orders of magnitude. Newly accelerated electrons are required.

Although various acceleration mechanisms have been proposed to explain the presence of these energetic electrons in SNRs, the general consensus for the past 30 years has been that the dominant process is DSA. The primary evidence is the rough agreement between mean SNR inferred electron index $s \sim 2$ and the simplest predicted test-particle power-law index, $s = 2$ for a compression ratio of 4. However, the considerable numbers of Galactic shell SNRs (about 40%; Green 2006) with $s < 2$ ($\alpha > -0.5$) pose a problem. These values of s could be explained with very low Mach-number shocks, but few remnants would be expected to have such slow shocks. It is possible that second-order Fermi (stochastic) acceleration plays a role (e.g., Ostrowski 1999). We can gauge its importance by examining acceleration rates. The acceleration time to energy E for stochastic acceleration (once particles are relativistic) scales as (Melrose 1974)

$$t_{\mathrm{acc}}(\mathrm{stoch}) \sim \left(\frac{\lambda_{\mathrm{mfp}}}{c}\right)\left(\frac{v_A}{c}\right)^{-2}, \tag{14}$$

where v_A is the Alfvén speed (in the downstream medium) and λ_{mfp} is the scattering mean free path. The rate for DSA scales as (e.g., Blandford & Eichler 1987; see below)

$$t_{\mathrm{acc}}(\mathrm{DSA}) \sim \left(\frac{\lambda_{\mathrm{mfp}}}{c}\right)\left(\frac{u_{\mathrm{sh}}}{c}\right)^{-2}, \tag{15}$$

where for the DSA time we have assumed a diffusion coefficient proportional to particle energy, which we take to be proportional to mean free path as is often done. The ratio of acceleration rates of the two processes then scales as

$$\frac{t_{\mathrm{acc}}(\mathrm{DSA})}{t_{\mathrm{acc}}(\mathrm{stoch})} \propto \mathcal{M}_{A2}^{-2}, \tag{16}$$

where $\mathcal{M}_{A2} \equiv u_{\mathrm{sh}}/v_A$ is the Alfvén Mach number of the downstream flow (because we expect the dominant turbulence to be in the downstream region). Because we expect the bulk postshock flow to be super-Alfvénic (equivalent to requiring that the postshock magnetic energy density not exceed the thermal energy density ρu_{sh}^2), under normal conditions we expect DSA to be more rapid. We shall assume henceforth that DSA is the primary mechanism producing energetic particles in SNR shocks. The problem of steep radio spectra may be resolved by nonlinear effects (see below).

The basic physics of diffusive shock acceleration has been ably reviewed by various researchers (Drury 1983, Blandford & Eichler 1987, Jones & Ellison 1991, Malkov & Drury 2001). The literature is vast and I provide only a brief summary here. In a collisionless shock wave, incoming particles have their velocities randomized not by binary collisions with particles of comparable mass, as in hydrodynamic shock waves, but by scattering from magnetic irregularities embedded in the downstream medium. A few of those particles may scatter back upstream and reflect from incoming inhomogeneities in the upstream medium. Because the particles interact with an effectively infinite-mass scatterer, their distribution does not rapidly settle down to a Maxwellian after a few scatterings, as is true for binary collisions, but instead develops a nonthermal power-law tail that extends to energies as high as is permitted by various loss processes: finite shock age or size, absence of irregularities of appropriate wavelength from which to scatter resonantly, or (for electrons only) radiative losses.

4.1. Particle Scattering

MHD: magnetohydrodynamic

We presume that particles scatter with a (probably energy-dependent) mean free path $\lambda_{\rm mfp}$. As the scattering is assumed to be resonant scattering from magnetic-field fluctuations, it is reasonable to express $\lambda_{\rm mfp}$ in terms of the particle gyroradius in the mean magnetic field r_g: $\lambda_{\rm mfp} \equiv \eta r_g = \eta(E/eB)$, where the second expression is appropriate for the extreme-relativistic limit $E \gg mc^2$. The factor η (not necessarily constant) is known as the gyrofactor; it is often assumed that the smallest physically reasonable mean free path is $\lambda_{\rm mfp} = r_g$ (Bohm limit), so that $\eta \geq 1$. In quasi-linear theory, in which diffusion is treated as a small perturbation to unperturbed gyromotion trajectories, η can be expressed in terms of the energy in resonant MHD fluctuations (those with wave vectors k satisfying the resonant condition of Equation 17 below): $\eta = (\delta B_{\rm res}/B)^{-2}$ (Blandford & Eichler 1987). The presumption of quasi-linear theory is then that $\delta B_{\rm res} \ll B$, or $\eta \gg 1$, though most researchers seem willing to consider values of η all the way to 1. We should note that constant η is then an assumption about the energy spectrum of magnetic fluctuations: that it is independent of wave vector (white noise). This is a fairly strong assumption.

The nature of the required fluctuations is not completely clear. A common presumption is that resonant scattering from circularly polarized MHD waves such as Alfvén waves, with frequency equal to the particle's gyrofrequency, will result in diffusion. With the gyrofrequency of a particle with Lorentz factor γ given by $\Omega_g = eB/\gamma mc$, the resonance condition is then

$$\Omega_g = \mathbf{k} \cdot \mathbf{v}, \tag{17}$$

so that more energetic particles require longer-wavelength waves for scattering. Various other types of scattering from plasma waves have also been considered in detail, but the most common prescription is that given above.

For $\mathbf{k}$ perpendicular to $\mathbf{v}$, no resonance is possible, and in the simple theory particles cannot scatter through a pitch angle of 90° (i.e., reverse directions). This subject has been debated extensively in the literature, and it is clear tht Nature finds a way for particles to reverse direction in scattering, through nonresonant interactions or many possible effects normally dominated by simple resonant scattering. The consensus assumption is that somehow particles manage to scatter through 90°.

The scattering is presumed to result in an effective mean free path $\lambda_{\rm mfp}$ scaling with the gyroradius, as above, and a diffusion coefficient (in principle varying with both position x and particle energy E)

$$\kappa(x, E) = \frac{1}{3}\lambda_{\rm mfp} c = \frac{1}{3}\eta\frac{Ec}{eB}. \tag{18}$$

This expression should apply to scattering along the direction of the magnetic field; that is, this κ is $\kappa_\parallel$. The nature of perpendicular or cross-field diffusion has been the subject of considerable discussion in recent years. One common assumption is that a particle on average is displaced one gyroradius perpendicular to field lines with every parallel scattering (e.g., Jokipii 1987). This gives rise to a perpendicular diffusion coefficent $\kappa_\perp = \kappa_\parallel/[1 + (\lambda_{\rm mfp}/r_g)^2] \equiv \kappa_\parallel/(1 + \eta^2)$. Then the diffusion coefficient in a direction making an angle θ with the magnetic field direction is a combination of parallel and perpendicular diffusion, and

$$\kappa = \kappa_\parallel \cos^2\theta + \kappa_\perp \sin^2\theta. \tag{19}$$

For application to shock acceleration, we are concerned with scattering along the shock normal. In this case, we define the angle between the shock normal and the upstream magnetic field to be the obliquity $\theta_{\rm Bn}$. (Shocks with $\theta_{\rm Bn} \sim 0$ are referred to as parallel shocks; if $\theta_{\rm Bn}$ is significantly different from 0, we refer to oblique shocks, and if $\theta_{\rm Bn} \sim 90°$, we have perpendicular shocks.) For perpendicular shocks, in which the gyromotion of particles carries them back and forth across the shock even in the absence of scattering, a process called shock drift acceleration is sometimes invoked, in which particles gain energy as a result of a grad B drift perpendicular to the shock surface and along the induced electric field $\mathbf{E} = -\mathbf{u_1} \times \mathbf{B}/c$. Jones & Ellison (1991) discuss this process (with references) and show that it is included in the convection-diffusion formalism discussed below.

4.2. Test-Particle Results

In the so-called test-particle limit in which the accelerated particles are energetically unimportant, simple well-known results can be obtained by solving a basic kinetic equation, the convection-diffusion equation for the momentum-space distribution function $f(x, p)$. For a plane shock, where u is the local fluid velocity,

$$\frac{\partial f}{\partial t} + u\frac{\partial f}{\partial x} - \frac{\partial}{\partial x}\kappa\frac{\partial f}{\partial x} = \frac{1}{3}\frac{\partial u}{\partial x}p\frac{\partial f}{\partial p}. \tag{20}$$

We presume any velocity of the scattering centers (MHD waves) with respect to the local fluid is much less than the particle speed. The well-known solution to this equation in the case of a shock is a power-law momentum distribution of accelerated particles. If the required far-upstream seed population is $f_1(p)$, the (constant in space) downstream distribution $f_2(p)$ is given by

$$f_2(p) = qp^{-q}\int_0^p dp'(p')^{(q-1)}f_1(p') \Rightarrow f_2(p) \propto p^{-q}, \quad \text{with} \quad q = 3r_{\text{comp}}/(r_{\text{comp}} - 1), \tag{21}$$

where r_{comp} is the shock compression ratio. This result is valid at all momenta. In the extreme-relativistic region $E \gg mc^2$, we have $E = pc$, so the energy distribution $N(E) \equiv 4\pi p^2 f(p)dp/dE$ is given by

$$N(E) = KE^{-s} \qquad \text{with} \quad s = (r_{\text{comp}} + 2)/(r_{\text{comp}} - 1). \tag{22}$$

For a strong shock in a medium with ratio of specific heats $\gamma = 5/3$, we have $r_{\text{comp}} = 4$ and therefore $s = 2$ implying a synchrotron spectral index $\alpha = -0.5$, close to the mean for Galactic SNRs. Of course, nothing can be said about the energy content in accelerated particles in the test-particle limit. Remarkably, these results are independent of the value or functional dependence of the diffusion coefficient: any mechanism causing diffusion of particles will produce shock acceleration. However, acceleration rates do depend strongly on κ, and consequently so do maximum energies producible by DSA.

The spatial distribution of particles for a plane shock is constant downstream; upstream the distribution drops exponentially,

$$f(x, p) = f(0, p)e^{-|x|u_1/\kappa}, \tag{23}$$

forming a particle precursor of characteristic width κ/u. The electron precursor could in principle be detectable through synchrotron radiation, as a synchrotron halo (see below).

We note that Equation 23 implies that if κ increases with momentum, higher-energy particles can diffuse further ahead of the shock than lower-energy ones. This means that at some distance $|x|$ ahead of the shock, one has a particle distribution that rises sharply at a momentum such that $\kappa(p) \sim u_1|x|$; lower-energy particles are not present. If this distribution impinges on an upstream cloud, it may give rise to a π^0-decay gamma-ray spectrum with a low-energy cutoff. This idea has been used in modeling sources with stronger TeV than GeV emission (see below).

4.3. Acceleration Rates and Maximum Energies

The length scale for particle diffusion ahead of the shock is κ/u, so the basic timescale for acceleration involving that length is κ/u^2 (cf. Equation 15). More formally, the time to accelerate a particle from momentum p_i to p is given by

$$\tau_{\rm acc} = \frac{3}{u_1 - u_2} \int_{p_i}^{p} \left(\frac{\kappa_1}{u_1} + \frac{\kappa_2}{u_2} \right) \frac{dp'}{p'}, \tag{24}$$

where the diffusion coefficient in general will have different values upstream and downstream. For a shock with compression ratio $r_{\rm comp}$, and using Equations 18 and 19, we obtain (for $p \gg p_i$)

$$\tau_{\rm acc}(p)(\text{parallel}) = \frac{3\kappa(p)}{u_1^2} \frac{r_{\rm comp}(r_{\rm comp}+1)}{r_{\rm comp}-1}, \tag{25}$$

assuming $\kappa_2 = \kappa_1$. If scattering is not isotropic, the shock obliquity markedly affects this result. Using the prescription above for cross-field diffusion, the acceleration time given in Equation 25 is shortened for $\theta_{\rm Bn} > 0$ by a substantial amount (Jokipii 1987). We can write $\tau_{\rm acc}(\theta_{\rm Bn}) = R_J \tau_{\rm acc}(\theta_{\rm Bn} = 0)$ (Reynolds 1998), with $R_J \leq 1$. For $\eta = 1$, $R_J(\theta_{\rm Bn})$ varies from 1 at $\theta_{\rm Bn} = 0$ to $1/(1 + r_{\rm comp})$ at $\theta_{\rm Bn} = 90°$, and R_J drops as η increases. For $\tan\theta > \eta$, i.e., a decreasing range of angles about 90°, $R_J \propto \eta^{-2}$ for large η, but outside that range R_J is roughly constant independent of η. For a spherical shock encountering uniform magnetic field, all obliquities are achieved somewhere on the shock surface, and the results can be complicated (Reynolds 1998).

The maximum energy to which particles can be accelerated by diffusive shock acceleration is clearly an important issue for cosmic ray origins and for high-energy emission from SNRs. Lagage & Cesarsky (1983) discussed this issue in the SNR context for the limitation of finite acceleration time available. This age limitation is similar to one obtained by considering the finite size of a spherical remnant (Berezhko 1996). This was generalized to include two more limitations: radiative losses (likely only important for electrons) (Webb, Drury & Biermann 1984) and a change in the availability of MHD waves above some wavelength, giving an abrupt increase in the diffusion coefficient above the corresponding particle energy, resulting in particle escape upstream (Reynolds 1998). In any of these cases, the form of the resulting distribution function should be well approximated as a (near) power-law with an exponential cutoff at some $E_{\rm max}$ (Drury 1991; Webb, Drury & Biermann 1984). For each of the three possible limitations mentioned, one can obtain an expression for $E_{\rm max}$: by equating the acceleration time to the lesser of the remnant age or the radiative-loss time, or, for the escape mechanism, by equating $E_{\rm max}$ to the energy of particles resonant with the maximum wavelength $\lambda_{\rm max}$ of MHD waves present. The results depend in detail on the shock compression ratio and obliquity (Reynolds 1998) but are roughly

$$E_{\rm max}(\text{age}) \sim 0.5 u_8^2 t_3 \, B_{\mu G} \, (\eta R_J)^{-1} \ \text{TeV}, \tag{26}$$

$$E_{\rm max}(\text{loss}) \sim 100 u_8 \left(\eta R_J B_{\mu G}\right)^{-1/2} \ \text{TeV}, \tag{27}$$

$$E_{\rm max}(\text{escape}) \sim 10 B_{\mu G} \lambda_{17} \ \text{TeV}, \tag{28}$$

where $u_8 \equiv u_1/10^8$ cm s^{-1}, $t_3 \equiv t/1000$ years, and $\lambda_{17} \equiv \lambda_{\rm max}/10^{17}$ cm. B in the equations above is the upstream magnetic field. There is no R_J dependence in the escape case. For a spherical remnant, maximum energies in the first two cases depend on obliquity through R_J (Reynolds 1998). At highly oblique shocks, Equations 26 and 27 suggest that for large η, higher $E_{\rm max}$ values than the Bohm limit allows may be achievable. However, this is likely to be unrealistic for several reasons: It is true only for highly oblique shocks, where it requires very low levels of turbulence, and it neglects injection physics (see below), which might limit the numbers of particles that might attain these energies (see Ellison, Baring & Jones 1995 for a fuller discussion). But these results show that in general one ought to expect that in typical SNR conditions, electrons and ions can easily achieve energies in the TeV range. Electrons of energy $E_{100} \equiv E/100$ TeV radiate the peak of their synchrotron emission at $h\nu_{\mathrm{peak}} \sim 2(B/10\ \mu\mathrm{G})E_{100}^2$ keV; even well above E_{max}, this can be significant because in the delta-function approximation in which each electron radiates all its energy at frequency ν_{peak}, the spectrum above ν_{max} drops only as $\exp[-(\nu/\nu_{\mathrm{max}})^{1/2}]$, and when calculated numerically with the exact single-particle emissivity, drops even slightly slower (Reynolds 1998). It should be borne in mind that E_{max} is merely a fiducial description for a rather gradual dropoff of emission; substantial synchrotron X-rays can be produced at frequencies considerably higher than $\nu_{\mathrm{max}}(E_{\mathrm{max}})$.

A more careful calculation of E_{max} (age) shows that it rises rapidly in pre-Sedov phases to the fiducial estimate of Equation 26, as the shock velocity remains high and deceleration is small. After a transition at a time of order t_{ch} (Equation 7), the rate of increase slows: $E_{\mathrm{max}}(\mathrm{age}) = 5E_{\mathrm{max}}(\mathrm{age})(t_{\mathrm{ch}})[1 - (t/t_{\mathrm{ch}})^{-0.2}]$. However, this maximum energy only applies to particles present since the earliest times; in addition, the injection of particles into the acceleration process is likely to have a substantial velocity dependence, so that slower shocks are less efficient. It is worth noting that if proton acceleration is age-limited and electron acceleration is loss-limited, older remnants may have a higher ratio than younger ones of π^0-decay luminosity at GeV-TeV energies to synchrotron luminosity at keV energies (Yamazaki et al. 2006). However, if acceleration efficiency drops with shock speed, the absolute levels may be quite low.

These are basically single-particle arguments, relevant for any shock geometry. A rather different argument, giving similar but not identical results, obtains a steepening in the entire accelerated-particle distribution for a spherical shock, as a result of the dilution of the upstream density as the volume increases for particles whose diffusion length is not negligible compared to the shock radius (Berezhko 1996). The steepening tends to begin at a slightly lower energy than the simple age limit of Equation 26 above, and is not exponential. The calculation involves several assumptions about geometry and postshock diffusion.

4.4. Nonlinear Effects

As mentioned above, to populate the Galactic cosmic-ray pool each SNR must provide of order 10^{48} erg in electrons, with a maximum energy of at least several TeV. If SNRs show the same accelerated ion/electron ratio of ∼70 seen in cosmic rays at Earth around 10 GeV (Gaisser 1990), over 10% of the total SNR energy must go into accelerated particles. Those particles will have a dynamical effect on the shock, so that the test-particle limit is no longer operative. A great deal of work in recent years has gone into modeling nonlinear shock acceleration, including the backreaction of accelerated particles (see references below and in the above-cited review articles). The most important effect is the deceleration of incoming fluid (in the shock frame) as accelerated particles diffuse ahead and scatter from incoming MHD fluctuations. **Figure 3** shows a schematic shock profile; in the shock frame, material enters at velocity u_1 far upstream ($x < 0$), and exits at u_2 downstream. The dotted line shows a test-particle result, with compression ratio $r_{\mathrm{comp}} = u_1/u_2$. The solid line shows the effects of nonlinear modification: the incoming flow is gradually slowed, though a thin transition (thermal subshock) still persists, in which the thermal gas is heated. The final compression ratio is larger than in the test-particle case, due to the inevitable escape of cosmic rays. (It should be noted that steady-state solutions of the convection-diffusion equation for the particle distribution are not possible for nonlinear models without some kind of particle escape. This can be argued physically if MHD waves are self-generated, as the first particles to reach a

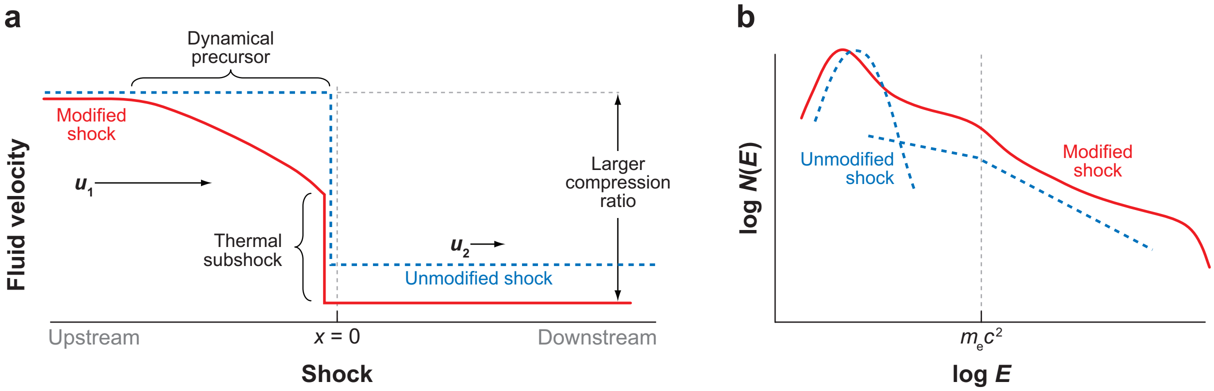

Figure 3

(*a*) Schematic shock profile. Dotted blue line, unmodified shock; solid red line, shock modified by accelerated particles. (*b*) Corresponding schematic particle energy distributions from unmodified shock (*dotted blue lines*) and modified shock (*solid red line*).

certain energy would not be scattered, but in the process of escaping would produce waves to scatter subsequent particles.) However, time-dependent calculations have also been done, as is described below.

The particle distribution produced by the modified shock profile may be understood qualitatively for particular assumptions about the energy dependence of diffusion. Assuming only that λ_{mfp} increases with particle energy, particles with higher energies will typically scatter farther ahead of the shock, where they will see an effectively higher compression ratio, and produce a locally harder spectrum. Thus we should expect a concave-up curvature to the accelerated-particle distribution, as sketched qualitatively in **Figure 3**. This result was first pointed out by Eichler (1979) and was quantified in Monte Carlo simulations (Ellison & Eichler 1984, Ellison & Reynolds 1991).

A second nonlinear effect concerns the MHD fluctuations required for scattering. Although such fluctuations are certainly present in the general interstellar medium, their amplitude (as deduced, for instance, from the diffusion of cosmic rays through the Galaxy; Achterberg, Blandford & Reynolds 1994) is far too low to keep particles of even radio-emitting energies near enough to SNR shocks to allow acceleration to high energies. Bell (1978) suggested that the accelerated particles themselves, streaming and scattering ahead of the shock, would excite MHD waves that would scatter subsequent generations of particles. The sharp rims seen in young SNRs at radio wavelengths can be used to bound the diffusion coefficient from below; Achterberg, Blandford & Reynolds (1994) infer substantially higher levels of turbulence, presumably self-excited by the accelerated particles themselves.

Self-generated waves have another effect: They can contribute to a feedback loop moving energy from fast particles back to the thermal plasma. Upstream MHD waves can damp through several mechanisms, heating the upstream gas (e.g., Bell 1978; Drury, Duffy & Kirk 1996). This mechanism may be responsible for the apparent absence in nature of the pure cosmic-ray dominated shock solution appearing in two-fluid models (see below) in which the entropy of the thermal gas does not increase at all.

Strong upstream turbulence may also have the effect of eliminating the distinction between parallel and perpendicular shocks. If the mean direction of the magnetic field is strongly fluctuating, the shock obliquity can vary strongly in both space and time. Such strong turbulence also implies $\delta B/B \sim 1$ and therefore $\eta \to 1$, so that the only difference in mean obliquity is the mean increase in magnetic-field strength for perpendicular shocks.

4.5. Injection

In test-particle calculations, a few particles are simply inserted into a pre-existing shock structure, and subsequently accelerated. In real shocks, some mechanism must exist for promoting a few particles to energies at which they see the shock (at least the thermal subshock) as a discontinuity; otherwise, they would simply be adiabatically heated as the fluid density rises continuously. This process is referred to as injection. The shock layer is expected to be a few thermal ion gyroradii thick, which means that ions need have only a few times the mean energy in order to have gyroradii considerably larger than the shock thickness. There are enough such particles in the exponential tail of the downstream Maxwellian; the process by which such particles scatter back ahead of the shock and become injected is referred to as thermal leakage. It is seen in Monte Carlo simulations (e.g., Ellison & Eichler 1984) and is generally accepted as the mechanism for ion injection. Electrons are another matter; because their initial gyroradii are smaller by the mass ratio, without some kind of boost they will never see the shock as a discontinuity. This difficulty is referred to as the injection problem. In the context of high-energy emission from SNRs, the process by which electrons begin the acceleration process may seem less than directly relevant; however, if that process has strong dependence on remnant parameters, such as upstream obliquity or neutral fraction, there may be significant consequences for X-ray to TeV emission.

Various plasma instabilities have been suggested to scatter thermal electrons up to energies at which their gyroradii are equal to ion gyroradii. This problem is currently unsolved; researchers often assume some fraction of electrons crossing the shock (typically of order 10^{-4}) is injected into the acceleration process. (See Malkov & Drury 2001 for an extensive discussion of the injection problem.) It is possible that high-energy observations may provide important constraints on models of electron injection.

4.6. Magnetic-Field Amplification

Observations of shocks in the heliosphere led Chevalier (1977) to suggest that shocks in supernovae and remnants could greatly amplify pre-existing magnetic fields. A specific mechanism for such amplification, a streaming instability of upstream cosmic rays in a parallel shock, has been advanced by Bell & Lucek (2001), with supporting numerical simulations in Lucek & Bell (2000). Observations in support of strong amplification are described in Section 7.1 below. Much is unknown about this possible process: the possible dependence on shock obliquity $\theta_{\rm Bn}$, the persistence (or not) of the strong oscillations in B as a DC field (nonzero mean), the dependence of the effect on shock speed or the presence of upstream neutrals. Work continues in these areas (e.g., Amato & Blasi 2006; Vladimirov, Ellison & Bykov 2006; Blandford & Funk 2007). The dependence of the age-limited maximum energy in Equation 26, $E_{\rm max}(\text{age}) \propto B$, means that much higher maximum energies than estimated by Lagage & Cesarsky (1983) would be possible with much stronger magnetic fields, so this issue is crucial for the analysis of high-energy emission from SNRs and for the whole question of cosmic-ray origin in general.

4.7. Calculations of Nonlinear Shock Acceleration

The first nonlinearity to be included in shock acceleration calculations was that of self-generated waves (Bell 1978). Bell (1978) found that if accelerated particles streaming ahead of the shock generated their own waves, their preshock distribution would not drop exponentially ahead of the shock, but much more slowly: roughly, $f(p) \propto 1/(x_0 + |x|)$, where x_0 is a preshock scale length inversely proportional to the accelerated particle distribution at the shock. However, the accelerated particles were still energetically unimportant test particles. Bell's treatment is notable for its probabilistic analysis, a good complement to the convection-diffusion equation approach of the other initial papers (Axford, Leer & Skadron 1977; Blandford & Ostriker 1978).

Dynamical nonlinearity, that is, including significant cosmic-ray pressure, was initially treated with two-fluid methods, in which cosmic rays and thermal gas are treated as coupled fluids with different ratios of specific heats (e.g., Drury & Völk 1981, and much later work described in the cited review articles). Early work considered diffusion coefficients either independent of, or varying only weakly with, energy. They tended to produce shock solutions in which all entropy was generated in the cosmic-ray fluid and the thermal gas was not heated at all beyond adiabatic compression. These cosmic-ray-dominated solutions were clearly inconsistent with the thermal X-rays emitted by almost all SNRs. Allowing the cosmic-ray fluid to pass energy back to the thermal gas through Alfvén wave generation and damping partially ameliorated this problem. Much more sophisticated versions of two-fluid models have been produced (see Malkov & Drury 2001 for an extensive review), but all suffer to some extent from a closure problem: As with the system of fluid equations, there are more variables than equations, and one needs additional closure relations among them to render the system soluble. Various specifications have been tried, including separately specified thermal and cosmic-ray adiabatic indices, a diffusive flux (i.e., a diffusion coefficient), an injection efficiency, a maximum energy, etc. However, without some input from a more fundamental kinetic theory, all these versions are subject to criticism, tending to exhibit pathologies of one type or another.

Various groups have augmented the two-fluid approach by simultaneously solving the convection-diffusion equation for the cosmic rays in order to calculate the moments of the cosmic-ray fluid self-consistently (e.g., Bell 1987; Berezhko, Elshin & Ksenofontov 1996; Falle & Giddings 1987; Kang & Jones 1995). In particular, Kang & Jones (1995) show that this approach, given appropriate choice of the closure parameters, produces results quite comparable to those from Monte Carlo and plasma simulations, discussed below. One significant model of this type (Berezhko & Ellison 1999) assumes a form for the particle distribution and parameterizes injection, obtaining a set of algebraic equations whose solutions compare well with simulations; it has been applied specifically to SNR modeling in Ellison, Decourchelle & Ballet (2004). An extensive series of papers by Berezhko, Völk, and coworkers applies the models of Berezhko, Elshin & Ksenofontov (1996) to various individual objects and astrophysical scenarios.

Numerical simulations of shock acceleration include a wide range of techniques. Monte Carlo methods (e.g., Eichler 1984, Ellison & Eichler 1984) are reviewed by Jones & Ellison (1991). At the expense of introducing ad-hoc scattering assumptions and the assumption of particle escape, these simulations can self-consistently determine particle spectra to high energies and overall flow dynamics. In hybrid simulations, the equations of motion are solved for ions, while electrons are treated as a fluid guaranteeing charge neutrality (e.g., Quest 1988). These simulations can show the formation of a collisionless shock as a magnetized fluid encounters a wall, and can follow the evolution of the shock and the production of fast particles. Studies of particle scattering and diffusion follow exact particle trajectories in turbulent magnetic fields (e.g., Giacalone & Jokipii 1994, Minnie et al. 2007). One unfortunate result of the latter studies is the finding that quasi-linear approximations for the diffusion coefficient and for cross-field diffusion (such as those in Equations 18 and 19) become less accurate for strong turbulence.

5. RADIATIVE PROCESSES

Four basic radiative processes are capable of producing emission from keV to TeV photon energies. Three are leptonic: synchrotron radiation, nonthermal bremsstrahlung, and IC scattering. The only radiative mechanism by which energetic hadrons might make themselves evident is photon emission by the decay of π^0 mesons produced in inelastic scattering of cosmic-ray ions from thermal protons. These four processes have been studied in the context of supernova remnants in detail by Sturner et al. (1997); Gaisser, Protheroe & Stanev (1998); Baring et al. (1999); Houck & Allen (2006); and others. **Figures 4** and **5** show typical calculations. I sketch the basic properties of each process below. Units are cgs unless otherwise indicated.

5.1. Synchrotron Radiation

Synchrotron radiation, though the only one of these four processes to be firmly identified in SNRs, is capable of producing photons only up to a few tens of keV. An electron with energy E radiates a continuous spectrum, rising as $\nu^{1/3}$ to a maximum

$$\nu_m = 1.82 \times 10^{18} E^2 B \text{ Hz} \tag{29}$$

or

$$h\nu_m = 1.93(E/100 \text{ TeV})^2 (B/10\mu\text{G}) \text{ keV} \tag{30}$$

and dropping exponentially with e-folding frequency $3.45\nu_m$ (Pacholczyk 1970). For an electron spectrum $N(E) = KE^{-s}$ electrons cm^{-3} erg^{-1}, the synchrotron emissivity in photons erg^{-1} cm^{-3} s^{-1} is given by (Pacholczyk 1970) *Erratum

$$\frac{dn_\gamma}{dE_\gamma dt dV} \equiv \frac{4\pi}{hE_\gamma} j_\nu = \frac{4\pi}{h} c_5(s)(8.31 \times 10^{-8})^{(s-1)/2} K B_\perp^{(s+1)/2} E_\gamma^{-(1+s)/2}, \tag{31}$$

where $c_5(s)$ is tabulated in Pacholczyk (1970) [$c_5(2.0) = 1.37 \times 10^{-23}$; $c_5(2.5) = 0.968 \times 10^{-23}$], and $B_\perp$ is the projection of the magnetic field on the plane of the sky. (j_ν is the form more commonly used in radio astronomy, in erg cm^{-3} s^{-1} Hz^{-1} sr^{-1}, where we have assumed an isotropic electron distribution.) This emissivity is very roughly proportional to the product of electron and magnetic energy densities. Because these two quantities cannot be deduced independently from observations of synchrotron emission alone, even basic properties of shock acceleration, such as overall efficiency, have been difficult to infer.

An electron loses energy to synchrotron radiation at the rate

$$-\dot{E} = 2\sigma_T c \gamma^2 \beta^2 \sin^2\theta \left(\frac{B^2}{8\pi}\right) = 1.57 \times 10^{-3} E^2 B^2, \tag{32}$$

where $\gamma \equiv E/m_e c^2$, $\beta^2 = 1 - 1/\gamma^2$, θ is the electron pitch angle, and σ_T is the Thomson cross section. The numerical constant is $\frac{\sigma_T c}{6\pi(m_e c^2)^2} = 1.57 \times 10^{-3}$ cgs. The numerical form of Equation 32 assumes $\beta \sim 1$ and averages over electron pitch angles. This equation can be trivially integrated to find the energy E of an electron of initial energy E_0 radiating in a constant magnetic field for time t:

$$E = \left(E_0^{-1} + 1.57 \times 10^{-3} B^2 t\right)^{-1}, \tag{33}$$

so that even an initially infinitely energetic electron, after time t, has energy $E_{\max}(t) = 637/B^2 t$ erg. The time to reach this energy, which is also the time to go from energy E to $E/2$, is $\tau_{1/2} = 637/B^2 E$ sec (again, averaging over electron pitch angles). We note that exactly analogous expressions to Equations 32 and 33 hold for IC scattering of radiation with energy density u_r, if we use an effective equivalent magnetic field with the same energy density: $B_r^2 \equiv 8\pi u_r$.

The enormous electron energies required for radiation in the X-ray band [$E = 72\,(h\nu/1 \text{ keV})^{1/2}\,(B/10\ \mu\text{G})^{-1/2}$ TeV] mean that this process exhibits the extreme high end of the electron spectrum. Observations show (see Section 6 below) that all known supernova remnants have X-ray fluxes below the extrapolation of their radio power-law spectra; at energies of

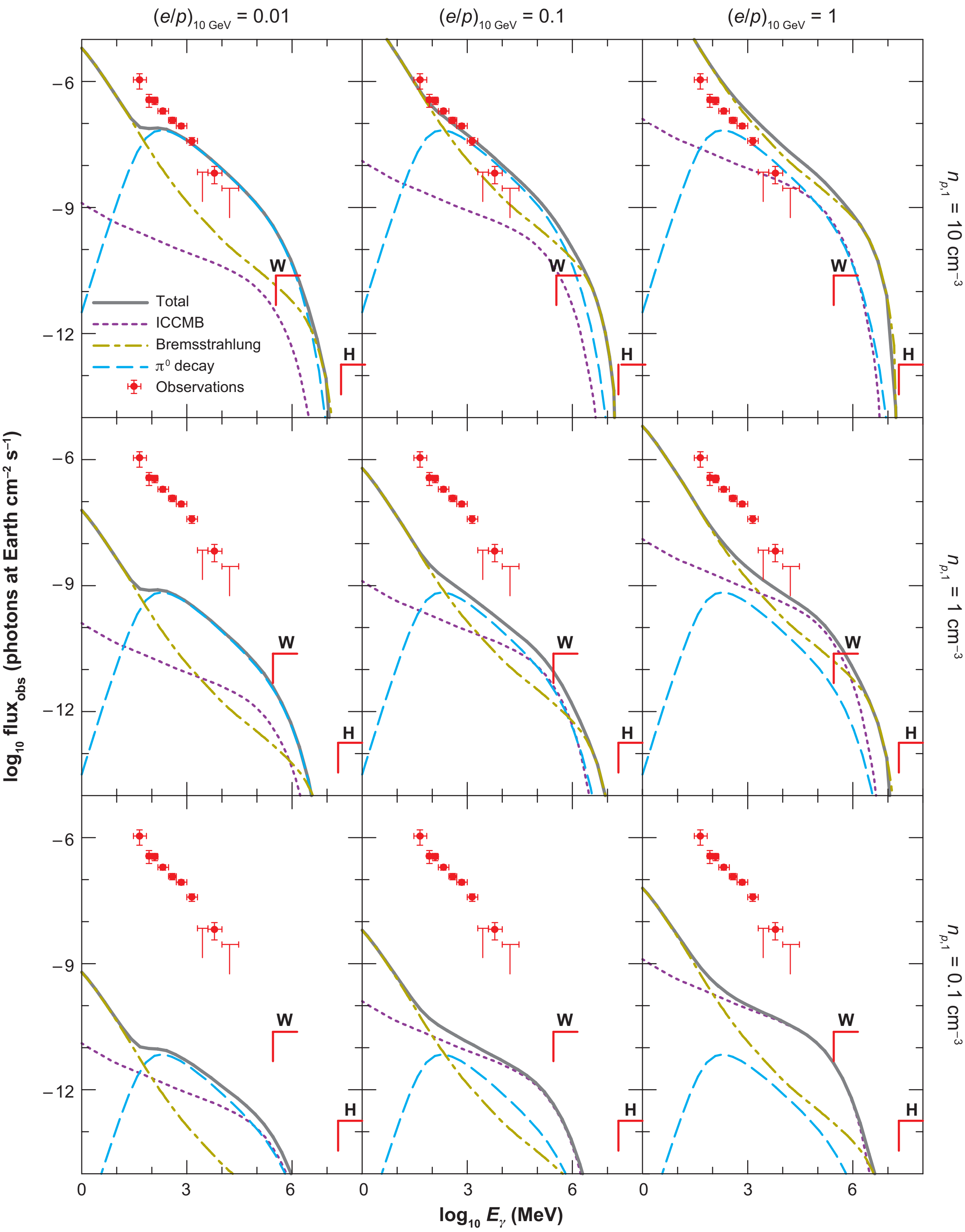
(e/p)10 GeV = 0.01
(e/p)10 GeV = 0.1
(e/p)10 GeV = 1
np,1 = 10 cm−3
np,1 = 1 cm−3
np,1 = 0.1 cm−3
log10 fluxobs (photons at Earth cm−2 s−1)
log10 Eγ (MeV)
−6
−9
−12
0
3
6
W
H
Total
ICCMB
Bremsstrahlung
π0 decay
Observations

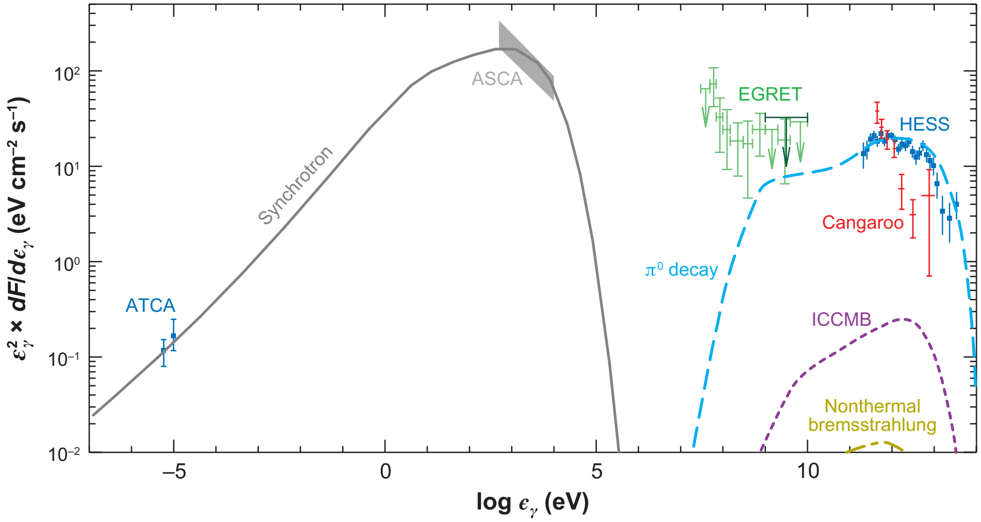

Figure 5

Model for the broadband integrated spectrum of G347.3-0.5 (Berezhko & Völk 2006). The spectrum has been multiplied by E^2. Green points, EGRET observations of nearby source 3EGJ1714-3857; dark green point, EGRET upper limit at location of G347.3-0.5.

10–100 TeV, the electron distribution is steepening as the maximum energy of the acceleration process is reached (or as subsequent radiative losses deplete electrons). An approximate form for the spectrum from an electron energy distribution that is not too far from a power-law can be obtained by approximating the single-electron emissivity as a delta-function at frequency ν_m. For the tail of an electron distribution with an exponential cutoff, this gives a volume emissivity $j_\nu \propto e^{-(\nu/\nu_m)^{1/2}}$. The delta-function approximation is fairly close to the exact calculation until $\nu/\nu_m \sim 30$, at which point the approximation begins to drop below the exact calculation and is about an order of magnitude below at $\nu/\nu_m = 100$.

Although highly ordered magnetic fields are relatively rare in the younger SNRs in which particle acceleration to high energies is taking place, it is worth remembering that the synchrotron emissivity of a volume element contains a factor $(\sin\theta)^{(s+1)/2}$, where θ is the angle between the local magnetic-field direction and the line of sight. This can be important in quantitative modeling of synchrotron morphologies; for instance, a substantial postshock component of radially directed magnetic field would depress the synchrotron brightness toward the center compared to that at the limbs.

5.2. Inverse-Compton Scattering

An extremely relativistic electron with Lorentz factor γ encountering a photon of not too high energy will upscatter it in energy by a factor of γ^2 and redirect it along the electron's direction of motion, with cross section $\sigma_T \equiv (8\pi r_e^2/3) = 6.65 \times 10^{-25}$ cm^2, where $r_e = 2.82 \times 10^{-13}$ cm is the

←

Figure 4

Examples of bremsstrahlung, inverse-Compton, and π^0-decay emission processes in the MeV-TeV range, for a range of ambient densities and electron/ion ratios (Baring et al. 1999). Dotted lines, ICCMB; dot-dashed, bremsstrahlung; dashed, π^0-decay; solid line, total. Symbols are observed fluxes and upper limits from IC 443.

classical electron radius. "Not too high" means having an initial energy $E_{\gamma i}$ much less than the electron's rest energy in the electron's rest frame, that is, the parameter $\Gamma_{\mathrm{K-N}} \equiv 4\gamma E_{\gamma i}/m_e c^2 \ll 1$. If this is not the case, the nonrelativistic (in the electron rest-frame) Thomson scattering is no longer recoilless, and the process is described by the Klein-Nishina cross section, which decreases below the Thomson value at high photon energies. An isotropic incident photon field $dn_\gamma(E_{\gamma i})/dV$ photons cm^{-3} erg^{-1} is scattered by a single electron of energy $E = \gamma m_e c^2$ to a spectrum of outgoing photons given by Jones (1968)

*Erratum

$$\frac{dn_{\gamma,e}}{dE_\gamma dt} = \frac{3}{4}\frac{\sigma_T c}{\gamma^2}\frac{m_e c^2}{E_{\gamma i}}\frac{dn_\gamma(E_{\gamma i})}{dV}dE_{\gamma i}\left[2q\ \ln\ q + (1+2q)(1-q) + \frac{\Gamma_{\mathrm{K-N}}^2 q^2(1-q)}{2(1+\Gamma_{\mathrm{K-N}}q)}\right], \quad (34)$$

where

$$q \equiv \frac{E_\gamma}{4E_{\gamma i}\gamma(\gamma - E_\gamma/m_e c^2)}. \quad (35)$$

We note that $0 \leq q \leq 1$; $q = 1$ gives the maximum photon energy.

Then the emergent photon spectrum is given by integrating Equation 34 over the electron spectrum [written here as $N(\gamma) = N(E)dE/d\gamma = N(E)m_e c^2$]:

$$\frac{dn_\gamma}{dE_\gamma dt dV} = \int N(\gamma)d\gamma \int \frac{dn_{\gamma,e}}{dE_\gamma dt}. \quad (36)$$

When Klein-Nishina effects are not important, the spectrum has the same shape as the electron spectrum; if the latter cuts off at some $E_{\max}$, the spectrum will cut off at a corresponding frequency $\nu_{\max} \sim \gamma^2\langle E_{\gamma i}\rangle$, where $\langle E_{\gamma i}\rangle$ is an average incident photon energy. Below the cutoff, the IC spectrum has the same slope as the synchrotron spectrum, with energy index $\alpha = (1-s)/2$.

The most likely source of seed photons for significant IC upscattering is the cosmic microwave background (CMB). Typical local radiation densities in the vicinities of SNRs are an order of magnitude less [see, for instance, estimates by Gaisser, Protheroe & Stanev (1998), though exceptions may exist]. For the CMB radiation, the photon spectrum $dn_\gamma(E_{\gamma i})/dV$ in Equation 34 is a blackbody at a temperature of $T = 2.73$ K:

$$\frac{dn_\gamma(E_{\gamma i})}{dV} = \frac{1}{\pi^2\hbar^3}\frac{E_{\gamma i}^2}{c^3}\left(e^{E_{\gamma i}/kT} - 1\right)^{-1}. \quad (37)$$

This subset of IC emission will be referred to as ICCMB.

5.3. Joint Synchrotron and ICCMB Modeling

The synchrotron and ICCMB emission spectra from a source are closely related, because they both depend on the extreme-relativistic end of the electron spectrum. The ratio of the two emissivities at some frequency, and the frequency ratio of the peaks, can be used to fix both the magnetic-field strength and the magnetic-field filling factor. The following discussion is based on appendix B of Lazendić et al. (2004), with some simplifications. For a simple homogeneous source filled with relativistic electrons and magnetic field (with a filling factor f_B), we can write down simple relations between the synchrotron emission and IC emission from CMB seed photons. We consider spectra plotted as νF_ν, so that both components rise with the same slope $1 + \alpha$ to peaks at frequencies ν_{ms} and ν_{mi}, respectively. Because Compton upscattering increases scattered photon energies by a factor $\sim 2\gamma^2$, a photon at the peak of the CMB spectrum with frequency 1.6×10^{11} Hz emerges at a frequency $\nu_i = 4.8 \times 10^{23} E^2$ Hz (with electron energy E in erg). From Equation 29, the magnetic field is fixed by the ratio of IC and synchrotron (SR) peak frequencies as

$$B = 9 \times 10^4 \left(\frac{\nu_{mi}}{\nu_{ms}}\right)^{-1} \text{ G}. \tag{38}$$

Suitable generalizations can be made to inhomogeneous sources whose turnovers are broadened (Ellison, Berezhko & Baring 2000).

We can write down the ratio of synchrotron to IC emissivity at a given frequency (assuming a power-law electron spectrum and neglecting Klein-Nishina effects, as is appropriate below the peak frequencies) from Equations 31 and 36 for the case of a thermal photon distribution at temperature T. The result is (Lazendić et al. 2004)

$$\frac{j_\nu(SR)}{j_\nu(IC)} \equiv [C(s)]^{-1}\, B^{(s+1)/2}, \tag{39}$$

where $C(s)$ is defined in Lazendić et al. (2004). In particular, $C(2.2) = 6.8 \times 10^{-14}$, $C(2.0) = 2.1 \times 10^{-14}$, and $C(1.7) = 3.6 \times 10^{-15}$.

Now the emitting volume of synchrotron radiation may be smaller than that of IC radiation, if magnetic field occupies a fraction $f_B \leq 1$ of the volume. Then the ratio of SNR to IC fluxes is smaller than the above ratio of emissivities by a factor f_B. We can invert the relation above to obtain

$$f_B = C(s)\frac{F_\nu(SR)}{F_\nu(IC)}B^{-(s+1)/2}. \tag{40}$$

Estimates based on similar considerations (but for $f_B \equiv 1$) were obtained by Aharonian & Atoyan (1999). These results reproduce the results of detailed model fitting to within factors of 25% for B and 2 for f_B.

5.4. Bremsstrahlung

Electrons of all energies emit bremsstrahlung photons in interactions with nuclei. Thermal electrons provide in this way the bulk of the thermal continuum; electrons with energies above the shock thermal energies of at most a few tens of keV will contribute a power-law spectrum with the same photon index Γ as their energy distribution index s. An electron with energy E emits photons up to about $E/3$, so the same TeV electrons that contribute keV synchrotron photons (mediated by the magnetic field) will contribute TeV bremsstrahlung photons (mediated by the ion density). Nonrelativistic electrons interacting with thermal electrons produce negligible radiation (strictly zero electric-dipole radiation), but at energies far above 1 MeV, electrons on nonrelativistic electrons emit about 86% as much radiation as they do interacting with ions (protons and 10% He by number) (Baring et al. 1999). Beginning around 100 MeV, bremsstrahlung photons are emitted by the same electrons that produce radio emission, so one expects a gamma-ray spectrum with $\Gamma \sim s \sim 2$. If the electron spectrum is $N_e(E)$ electrons cm^{-3} erg^{-1}, and it encounters protons with density n_H cm^{-3}, Gaisser, Protheroe & Stanev (1998) give a rough estimate of

$$\frac{dn_\gamma}{dE_\gamma dt dV} \sim 7 \times 10^{-16} n_H\, N_e(E_\gamma) \text{ photons erg}^{-1}\text{ s}^{-1}\text{ cm}^{-3}. \tag{41}$$

A single electron encountering a gas of H and He radiates a photon spectrum

$$\frac{dn_{\gamma,e}}{dE_\gamma dt} = v_e[(n_H + 4n_{\rm He})\sigma_{e-p}(E, E_\gamma) + n_e\sigma_{e-e}(E, E_\gamma)] \text{ photons s}^{-1}\text{ erg}^{-1}. \tag{42}$$

For electron-ion bremsstrahlung, this expression assumes the Bethe-Heitler cross section with $Z = 1$ for σ_{e-p}; the explicit 4 for He was inserted in Equation 42. Analytic expressions for σ_{e-e} are given in the appendix of Baring et al. (1999). The full photon spectrum is obtained by integrating Equation 42 over the electron distribution.

5.5. π^0 Decay

This process has been discussed in connection with supernova remnants for decades (e.g., Blandford & Cowie 1982). Several more detailed applications using the results of DSA were presented in 1994 (Drury, Aharonian & Völk 1994; Naito & Takahara 1994). Above the π-creation threshhold of 1.2 GeV, the cross section for $p + p \to$ anything is roughly just the geometrical cross section of a proton, $\sigma \sim (10^{-13}\ \mathrm{cm})^2 \sim 10^{-26}\ \mathrm{cm}^2$, varying little with proton energy (Dermer 1986b). Almost all the products are pions, and one-third of those are π^0s. They are isotropically emitted in the target rest frame, so the energy dependence in the lab frame is just given by relativistic kinematics.

The secondary π^0 spectrum Q_{π^0} (pions cm^{-3} s^{-1} erg^{-1}) produced by the interaction of an incident flux of energetic protons $\mathcal{J}_p(E)$ with gas with a thermal proton density of n_H cm^{-3} is

$$Q_{\pi^0}(E_\pi) = 4\pi n_H \int_{E_{\min}(p)}^{\infty} dE_p \mathcal{J}_p(E) \frac{d\sigma(E_p, E_\pi)}{dE_\pi}. \tag{43}$$

The differential cross section $d\sigma(E_p, E_\pi)/dE_\pi$ involves details of strong-interaction physics. Approximate analytical expressions were derived by Dermer (1986a). The minimum energy required to produce a pion with energy E_π is given by

*Erratum

$$E_{\min}(p) = m_p c^2 + 2E_\pi + m_\pi c^2 \left(2 + \frac{m_\pi}{2m_p}\right) \tag{44}$$

An isotropic distribution of π^0s will decay through $\pi^0 \to \gamma + \gamma$ to produce a photon spectrum peaking at energy $m_\pi/2 = 68$ MeV and dropping symmetrically on either side. The higher the energy of the π^0s, the broader the peak. The photon spectrum is given by

$$\frac{dn_\gamma}{dE_\gamma dt dV} = 2f \int_{E_{\min}(\pi)}^{\infty} dE_\pi \frac{Q_{\pi^0}(E_\pi)}{p_\pi}, \tag{45}$$

where p_π is the pion momentum. The minimum pion energy required to produce a photon of energy E_γ is $E_{\min}(\pi) = E_\gamma + (m_\pi^2 c^4/4E_\gamma)$. The factor f in Equation 45 is a factor accounting for gamma rays produced from He and heavier elements in both projectile and target populations. Dermer (1986b) estimates $f = 1.45$. This scaling assumes that the energy dependence of pion production by heavier projectiles and targets is the same as that for protons on protons, though this is clearly an approximation.

The photon production at a given energy is dominated by protons near threshold for production of the appropriate pions, for the steep spectra we anticipate, so the spectrum from an arbitrary distribution of energetic protons turns on around 70 MeV and then follows the spectral shape of the proton distribution. If that distribution $N(E_p)$ protons erg^{-1} cm^{-3} changes slowly with energy, we can estimate

$$\frac{dn_\gamma}{dE_\gamma dt dV} \sim 10^{-16} n_H\, N(E_\gamma) \text{ photons erg}^{-1}\ \text{s}^{-1}\ \text{cm}^{-3} \tag{46}$$

*Erratum

E in erg: (Gaisser, Protheroe & Stanev 1998). Various Monte Carlo programs are available to calculate the cross sections in detail (see references in Gaisser, Protheroe & Stanev 1998). For power-law spectra, the normalized integrated gamma-ray emissivity $q_\gamma(\geq 100\ \text{MeV}) \cong 5 \times 10^{-14}$ cm^3 s^{-1} erg^{-1} (H atom)$^{-1}$ (Dermer 1986b; Drury, Aharonian & Völk 1994), relatively independent of the power-law index (between 2.1 and 2.7 at least). The integrated gamma-ray yield $Q_\gamma(\geq 100\ \text{MeV})$ (ph cm^{-3} s^{-1}) is then given by $q_\gamma(\geq 100\ \text{MeV})\, n_H\, u_{\rm rel}$, where $u_{\rm rel}$ is the energy density in relativistic protons.

6. OBSERVATIONS

6.1. Instruments

3EGC: Third EGRET Galactic-Plane Source Catalog

The observational tools used to study supernova remnants at high energy fall cleanly into three categories: X-ray (up to about 10 keV, and in a few cases to 20 or 30); MeV-GeV (from about 0.1 MeV to 100 GeV), and TeV (from 0.3 TeV up). The first two are exclusively space-based, whereas the last involves ground-based techniques. The soft X-ray part of the spectrum has been the subject of intense study by exceptional instruments in recent years. The ROSAT All-Sky Survey provides an excellent reference for the energy range 0.1–2 keV, with angular resolution (S/N permitting) of order 30 arcsec. The field of nonthermal X-rays from SNRs really became established with the ASCA satellite, with a spatial resolution of better than an arcminute and energy range from ∼0.3 keV up to 9 keV. However, the combination of angular resolutions of 0.5–15 arcsec and CCD energy resolutions $E/\Delta E \sim 10-15$, embodied in *Chandra* and *XMM-Newton*, has revolutionized our understanding of the X-ray sky. These instruments cover the energy range from about 0.2 to 8 keV. Higher energies, up to several tens of keV, can be reached by RXTE, though with poor angular resolution, and by the Hard X-ray Detector (HXD) aboard *Suzaku*.

These energy ranges overlap the lowest energies observable by several gamma-ray missions. The OSSE instrument aboard the *Compton Gamma-Ray Observatory* (CGRO) had sensitivity down to a few tens of keV, but the primary MeV-GeV instrument for SNR studies (before GLAST) has been the EGRET spark-chamber instrument aboard CGRO. EGRET was sensitive to gamma rays between 30 MeV and 20 GeV; the third EGRET Catalog (3EGC; Hartman et al. 1999) included 74 unidentified sources within 10° of the Galactic plane at energies above 100 MeV. Positional uncertainties depend on source strength and range from a few arcmin to over a degree, and few solid identifications with SNRs have been made. EGRET provided essentially the only window on this part of the electromagnetic spectrum with better than a few degrees angular resolution, until the launch of the INTEGRAL satellite in 2002. INTEGRAL's primary instrument IBIS is sensitive from about 17 keV up to 10 MeV; it also carries X-ray monitors (Jem-X), operative from about 3 keV. The coded-mask imaging technique allows localization of point sources to about 12 arcmin but is not ideal for the study of extended sources. The Large Area Telescope (LAT) aboard GLAST operates between about 100 MeV and 100 GeV with a sensitivity about two orders of magnitude greater than EGRET, with source localization to an arcminute or so.

Above a few hundred GeV, ground-based optical techniques become possible. Photons at these energies incident on the top of the atmosphere produce air showers, which result in easily detectable flashes of Čerenkov light. The air-Čerenkov technique has now been used successfully in a series of instruments (IACTs, or Imaging Air Čerenkov Telescopes) from the pioneering Whipple 10-m Telescope in 1968, to HEGRA, CAT, CANGAROO, MAGIC, and HESS. These instruments discriminate photon from particle-initiated showers on the basis of the geometric appearance of the shower as imaged by one (e.g., Whipple or MAGIC) or several (CANGAROO-III, HESS) optical telescopes. Angular resolutions depend on the shower elevation, but can reach 10 arcmin. A related instrument, MILAGRO, uses a water-Čerenkov detector to study similar showers, thus not requiring dark skies.

As of this writing, fewer than ten SNRs show unmistakable evidence for nonthermal emission at or above X-ray photon energies. I discuss each of these individually below.

6.2. SN 1006

SN 1006 (see **Figure 1**) remains the archetypical X-ray-synchrotron-dominated shell SNR. The integrated spectrum, determined with ASCA between 0.6 keV and 10 keV, shows weak line features of helium-like Mg and Si, but is dominated by nonthermal emission; fitting with a shock plus power-law requires a photon index of $\Gamma = 2.5 \pm 0.15$ (Dyer et al. 2001). Similar values are found in the bright rims from *Chandra* observations (Long et al. 2003). The most complete spectral/spatial observations reported to date have been done with the *XMM-Newton* satellite (Rothenflug et al. 2004). These researchers find the bright limbs to show featureless spectra well described by emission from an exponentially cut off power-law (model srcut; Reynolds & Keohane 1999), with rolloff photon energies of 0.1 keV to 4 keV. The rolloff energy is related to the *e*-folding energy of the exponential cutoff, $E_{\rm max}$, by

$$E_{\rm max} = 39 \left(\frac{h\nu_{\rm rolloff}}{1\ {\rm keV}}\right)^{1/2} \left(\frac{B}{10\ \mu{\rm G}}\right)^{-1/2}\ {\rm TeV}, \tag{47}$$

so the highest rolloffs found by Rothenflug et al. (2004) imply $E_{\rm max} \sim 80$ TeV, consistent with earlier ASCA observations (Dyer et al. 2001, Koyama et al. 1995).[1] The rolloff energies vary systematically with azimuth; in the NW and SE quadrants, where nonthermal radio emission is weaker, there are only upper limits. The rolloff energies also drop as one moves behind the shock. Dyer et al. (2001) fit the nonthermal spectrum with a particular model (sresc) based on calculating a maximum electron energy as a function of shock obliquity, and evolving an assumed power-law with that cutoff energy behind the shock, taking account of radiative and adiabatic losses (Reynolds 1998). The model assumed Sedov evolution into a uniform medium, appropriate for a Type Ia remnant. That model was able to account for the observed synchrotron spectrum assuming the maximum energy was due to particle escape; the implied maximum wavelength of MHD waves was about $10^{17}(B_1/3\ \mu{\rm G})^{-1}$ cm, where B_1 is the upstream magnetic field, assumed to be uniform.

In principle, a featureless power-law spectrum could be produced by other mechanisms. A power-law energy distribution of electrons will produce a power-law bremsstrahlung spectrum (Section 5.4), but electrons with energies of a few keV, whether drawn from a power-law or a quasi-Maxwellian distribution, will still excite lines. The most elaborate attempt at a nonsynchrotron model for the featureless X-ray spectrum of SN 1006 was produced by Laming (1998) using bremsstrahlung behind a reverse shock into pure carbon ejecta, fully stripped to suppress lines. Laming reports that the required conditions make the model infeasible for SN 1006, although similar models might be more relevant for X-ray emission from other remnants. Other processes such as IC emission would produce far harder spectra than the $\Gamma \sim 2.5$ observed.

One prediction of the synchrotron model is that the nonthermal spectrum should be steepening. In contrast, the lowest-energy nonthermal electrons ought to have an energy distribution that is either a power-law or actually hardening with energy due to nonlinear shock modification (Section 4), so nonthermal bremsstrahlung would produce a straight or convex-up spectrum. The synchrotron prediction has been confirmed with observations by RXTE (Dyer et al. 2001, Kalemci et al. 2006). SN 1006 was not detected by EGRET; the upper limits from the 3EGC in the vicinity of SN 1006 appear to be roughly $F(>100\ {\rm MeV}) < 2 \times 10^{-7}$ ph cm^{-2} s^{-1}.

A deep observation with HESS failed to detect SN 1006 with a 99.9%-confidence upper limit to the integrated flux above 0.26 TeV of 2.4×10^{-12} photons cm^{-2} s^{-1} (Aharonian et al. 2005). This upper limit provides significant constraints on any model for the TeV emission. The high-energy emission from SN 1006 has been modeled in detail by various investigators (Reynolds 1998; Ellison, Berezhko, & Baring 2000; Dyer et al. 2001; Berezhko, Ksenofontov & Völk 2003). The HESS upper limit (Aharonian et al. 2005) requires both a substantial magnetic field, $B \gtrsim 25\ \mu$G, to

[1]Equation 47 is the corrected version of a similar but incorrect equation in Reynolds & Keohane (1999).

suppress ICCMB for the observed synchrotron fluxes, and a low thermal-gas density, $n_0 \lesssim 0.1\ \mathrm{cm}^{-3}$ (Ksenofontov, Berezhko & Völk 2005), to suppress π^0-decay emission.

The X-ray morphology of SN 1006 also suggests that the magnetic field strength might be significantly stronger just behind the shock than typically assumed. Bamba et al. (2003b) pointed out that the *Chandra* image showed extremely thin filaments, perhaps unresolved in some cases at the 1 arcsec level. These thin rims have also been observed in other remnants (see below).

6.3. G347.3-0.5 (RX J1713.7-3946)

G347.3-0.5 was identified as an SN 1006-like remnant by Koyama et al. (1997) based on its featureless X-ray spectrum in ASCA Galactic Plane Survey data. They estimated a distance of order 1 kpc based on their absorption determination of $N_H \sim 5 \times 10^{21}\ \mathrm{cm}^{-2}$. Subsequent pointed observations with ASCA (Slane et al. 1999) showed that all parts of the remnant had comparable power-law indices ($\Gamma \sim 2.41 \pm 0.05$); lines were nowhere evident, and Slane et al. (1999) put an upper limit on the preshock thermal-gas density of $n_0 \lesssim 0.7\, d_{\mathrm{kpc}}^{-1/2}\ \mathrm{cm}^{-3}$, where d_{kpc} is the distance in units of kiloparsecs. Slane et al. (1999) also presented radio data showing arcs of emission in the NW quadrant, not highly correlated with X-ray features. Infrared and CO data indicated substantial quantities of cool material around the NW.

Subsequent observations with *XMM-Newton* (Cassam-Chenaï et al. 2004b) confirmed the basic results of Slane et al. (1999), but quoted a larger variation in Γ (1.8–2.6), with steeper values in the interior and where the shock appears to be interacting with CO clouds. Cassam-Chenaï et al. (2004b) argued convincingly for an association with those clouds based on higher absorption near the clouds; the CO velocities imply a distance of 1.3 ± 0.4 kpc. Hiraga et al. (2005) used *XMM-Newton* data to improve the limit on the remnant's thermal-gas density to $n_e \sim 0.1 d_{\mathrm{kpc}}^{-1/2}$ cm^{-3}. Higher resolution X-ray observations with *Chandra* (Uchiyama, Aharonian & Takahashi 2003; Lazendić et al. 2004) show that the bright NW corner is composed of very thin filaments parallel to the shock edge, which do not correlate extremely well with radio structures seen by ATCA (Lazendić et al. 2004).

The remnant contains an X-ray point source, 1WGA J1713.4-3949, whose properties are similar to central compact objects (CCOs) in other SNRs (Cassam-Chenaï et al. 2004b), thus typing G347.3-0.5 as the remnant of a core-collapse SNR.

G347.3-0.5 is near, but outside, the error box of the EGRET source 3EG J1714-3857. Butt et al. (2001) argued for an association, with protons accelerated in the shock wave of G347.3-0.5 diffusing into a nearby molecular cloud roughly coincident with the EGRET source, and there producing π^0-decay GeV emission. They cited an unusually high ratio of molecular-line intensities to argue for interaction with the CO cloud. In any case, most researchers have used the observed flux of 3EG J1714-3857 as an upper limit on any emission coincident with the X-ray shell of G347.3-0.5 itself.

G347.3-0.5 was detected in TeV gamma rays with the CANGAROO instrument; Enomoto et al. (2002) quote a spectrum with power-law photon index $\Gamma = 2.8 \pm 0.3$. They used broad-band modeling similar to that done for SN 1006 to conclude that only a π^0-decay model could describe the data, especially given the constraining EGRET upper limit. Observations with HESS (Aharonian et al. 2007b) gave about the same differential flux at 1 TeV, but a somewhat flatter spectral shape: a power-law of $\Gamma \sim 2.2 \pm 0.2$ around 1 TeV, but steepening slightly (see **Figure 6**). Aharonian et al. (2007b) also presented an image based on three years of data, with angular resolution of about 4 arcmin. The image (**Figure 6**) correlates remarkably well with the X-ray image.

Broadband modeling (Lazendić et al. 2004, Aharonian et al. 2007b) has shown that the integrated spectrum of G347.3-0.5 from radio to TeV energies could be fairly well described by either

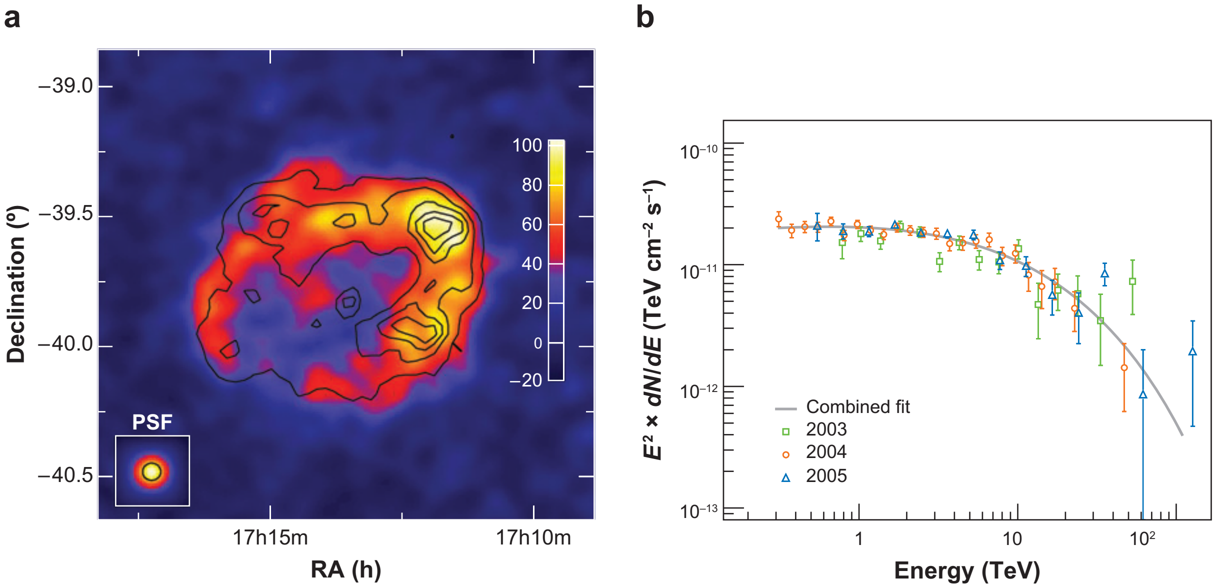

Figure 6

(*a*) TeV image of G347.3-0.5 with the HESS instrument (Aharonian et al. 2007b). Contours: ASCA 1–3 keV image. (*b*) TeV spectrum (Aharonian et al. 2007b).

an ICCMB or a π^0-decay model, though neither model was completely convincing. The ICCMB model requires a very low filling factor of magnetic field to avoid drastically overpredicting the keV emission, whereas a π^0 model (e.g., Berezhko & Völk 2006, **Figure 5**) requires a larger density of target atoms than seems present based on the X-ray limits; the excellent spatial correlation between synchrotron X-rays and TeV emission argues against invoking interaction with external material.

Uchiyama et al. (2007) report time variability of the X-ray emission from G3473.3–0.5 on a timescale of years, from *Chandra* observations in 2000, 2005, and 2006. Features on scales of about 10 arcsec were seen to brighten and to fade. Uchiyama et al. interpret these changes as owing to real-time electron acceleration, for brightening, and radiative losses, for fading. The required magnetic fields in both cases are of order 1 mG for this interpretation, though other interpretations of the observed changes are possible.

6.4. G266.2-1.2 (Vela Jr.)

This large, faint remnant was discovered in ROSAT observations of the Vela SNR (Aschenbach 1998). Above 1.2 keV, a clear shell was found superimposed on the SE quadrant of the large ($\sim 5°$) Vela remnant. The new remnant, itself about 2° in diameter, has ROSAT designation RX J0852-4622 and Galactic designation G266.2-1.2, but has come to be known familiarly as "Vela Jr." Like SN 1006 and G347.5-0.3, G266.2-1.2 shows narrow filaments in X-rays (Bamba, Yamazaki & Hiraga 2005). A great deal of excitement was generated by the early report of detection of a 1.156-MeV nuclear gamma-ray line with 5.6 σ significance with the COMPTEL instrument aboard CGRO (Iyudin et al. 1998). This line results from the decay of ^{44}Ti (half-life 62 years), presumably synthesized in the supernova. From the observed flux, and assuming a typical SN yield of ^{44}Ti of $5 \times 10^{-5}\ M_\odot$, Iyudin et al. (1998) inferred an SNR age of about 680 years, but required a very small distance, about 200 pc, placing the remnant in front of the Vela SNR. The possibility of the discovery of what would be the fourth youngest known SNR produced considerable interest. However, careful consideration of the COMPTEL data (Schönfelder et al. 2000) reduced the confidence level of the detection to $(2-4)\sigma$, and a considerably larger distance is given by other determinations (see below).

The decay chain from ^{44}Ti leads to ^{44}Sc, which produces the 1.16-MeV line in decaying to ^{44}Ca. Electron-impact excitations of either ^{44}Ti or ^{44}Sc can produce a line at about 4.5 keV. The electron capture producing ^{44}Sc should be followed by a radiative cascade, with a K-shell transition at 4.1 keV. This feature was reported by Tsunemi et al. (2000) but not confirmed by Slane et al. (2001).

G266.2-1.2 was unearthed from Parkes 2.4-GHz radio survey data (Combi, Romero & Benaglia 1999), and shown to have a nonthermal radio spectral index, though with large errors. Combi, Romero & Benaglia (1999) showed that the featureless spectrum reported by Aschenbach (1998) could be reasonably explained as the synchrotron-loss-steepened tail of this same radio spectrum. The radio spectral index determination was improved to $\alpha = -0.4 \pm 0.1$ in the northern shell by Duncan & Green (2000). Subsequent X-ray observations with ASCA (Tsunemi et al. 2000, Slane et al. 2001) confirmed that the X-ray spectrum is almost completely free of lines, except for features that could be associated with the overlapping Vela remnant. Slane et al. (2001) quote power-law fits with photon index $\Gamma = 2.6 \pm 0.2$, and also give an upper limit on the thermal-gas density of $n_0 \lesssim 0.03$ cm^{-3} in the bright northern rim. Slane et al. (2001) obtain a considerably larger absorbing column density, $N_H \sim (1-4) \times 10^{21}$ cm^{-2}, than characterizes the Vela remnant, suggesting a considerably larger distance than Vela's ~300 pc. The absorption and nonthermal spectra were confirmed by observations with *XMM-Newton* (Iyudin et al. 2005), but the latter researchers also reported a weak line at 4.45 ± 0.05 keV, which they associate with electron-impact excitations of ^{44}Ti and ^{44}Sc. The existence of the lines at 4.1 and 4.45 keV remains controversial.

G266.2-1.2 was detected in TeV gamma rays by both the CANGAROO (Katagiri et al. 2005) and HESS (Aharonian et al. 2007a) instruments, with roughly consistent results. The HESS significance image is shown in **Figure 7**. They find a spectrum well-fit by a power-law with photon index $\Gamma = 2.1 \pm 0.3$. Their flux is reasonably well described by either an ICCMB model or a π^0-decay model; in the latter case, for a distance of 200 pc and making simple assumptions, a total energy in relativistic protons of about 10^{49} erg would be required (assuming an ambient thermal-gas density of 1 cm^{-3}). At this point, the TeV data do not allow a discrimination.

G266.2-1.2 also possesses a central X-ray point source (Pavlov et al. 2001), probably a CCO. It does not have an associated PWN. Its presence does allow the classification of G266.2-1.2 as a core-collapse remnant.

6.5. Other Historical Shells

The broadband spectra of Kepler (SN 1604), Tycho (SN 1572), and G11.2-0.3 (SN 386; Roberts et al. 2003), as well as Cas A (not strictly historical but evidently an SN around 1680 AD), are all dominantly thermal below about 8 keV. However, all but G11.2-0.3 show evidence for a hard power-law tail to about 20 keV based on RXTE data (Allen et al. 1997; Allen, Gotthelf & Petre 1999). Cas A has been observed to 80 keV by BeppoSAX (Favata et al. 1997) and to 100 keV by the OSSE instrument on CGRO (The et al. 1996), showing a fairly straight power-law with photon index $\Gamma = 2.95(+0.09, -0.5)$ (Favata et al. 1997). Because these energies are above those at which any astrophysically common elements can produce lines, the emission could be either nonthermal bremsstrahlung or synchrotron radiation, though naïve models predict that the former process should flatten to higher energies, whereas the latter steepens. Allen et al. (1997) find a steepening in Cas A's hard X-ray spectrum and argue for synchrotron radiation, while Vink &

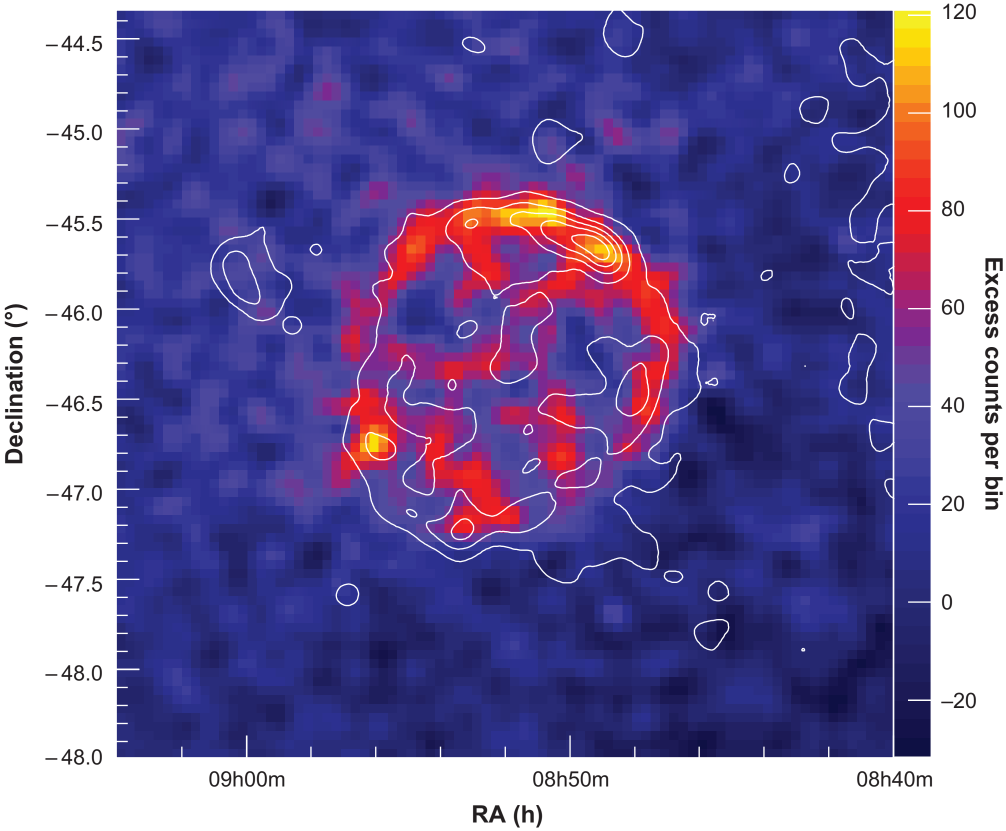

Figure 7

A fourth significance image in TeV photons of G266.2-1.2, in color (Aharonian et al. 2007a). White lines, X-ray contours (Aschenbach 1998).

Laming (2003) find that both processes may be required. Observations of G11.2-0.3 with RXTE have not been reported, but an analysis of *Chandra* observations (Roberts et al. 2003) required the presence of both thermal and nonthermal spectral components in the shell. Roberts et al. (2003) used the srcut synchrotron model to describe the nonthermal part, and quoted a rolloff frequency of $(1.8 \pm 0.1) \times 10^{16}$ Hz, implying e-folding energies of $11(B/10\ \mu\mathrm{G})^{-1/2}$ TeV.

Cas A, Kepler, and Tycho, like SN 1006, all show small-scale features that are probably synchrotron emission. Thin rims in Cas A probably distinguish the blast wave (Gotthelf et al. 2001); their spectra show lines, but require in addition a nonthermal component well described by a power-law with $\Gamma \sim 2$. Nonthermal emission from the thin rims in Tycho was first discussed by Hwang et al. (2002). Bamba et al. (2005) collected *Chandra* data for Cas A, Kepler, and Tycho, as well as the possibly historical remnant RCW 86, discussed in the next section. They found the spectra of the thin features to be characterized by similar parameters to those for SN 1006, and discussed a possible phenomenological correlation among filament width, rolloff frequency, and remnant age. However, not all synchrotron emission occurs in thin rims; RCW 86 is a counterexample (Rho et al. 2002).

None of the historical shells has been detected by EGRET. Upper limits vary with Galactic position but are comparable to those for SN 1006, at several $\times 10^{-7}$ photons cm^{-2} s^{-1} integrated above 100 MeV. At TeV energies, Cas A has a reported 5σ detection with the HEGRA CT-system, with $F(>1 \text{ TeV}) = (5.8 \pm 1.2_{\text{stat}} \pm 1.2_{\text{syst}}) \times 10^{-13}$ photons cm^{-2} s^{-1}, with a photon index between 1 TeV and 10 TeV of $\Gamma = -2.5 \pm 0.4_{\text{stat}} \pm 0.1_{\text{syst}}$ (Aharonian et al. 2001a). For Tycho, several instruments have reported nondetections, of which the most stringent is from HEGRA, with a flux $F(>1 \text{ TeV}) < 5.8 \times 10^{-13}$ photons cm^{-2} s^{-1} (3σ) (Aharonian et al. 2001b, who also reference earlier results). Sinitsyna et al. (2005) claim a detection of Tycho with the SHALON air-Čerenkov telescope in Tien-Shan, at the level of $F(> 0.8 \text{ TeV}) = 5.2 \times 10^{-13}$ photons cm^{-2} s^{-1}. A power-law was fit to the spectrum with index $\Gamma = -2.14 \pm 0.06$ between 0.8 TeV and 20 TeV. These results are barely consistent with the HEGRA upper limit. No TeV gamma-ray detections have been reported for Kepler or for G11.2-0.3.

6.6. RCW 86

RCW 86 (G315.4-2.3) has a complete radio shell with diameter about 40 arcmin. It has been argued to be the remnant of the supernova of 185 AD (Vink et al. 2006). ASCA observations of the SW quadrant revealed surprisingly weak lines. However, a combination of a plane shock and an srcut model described the *Chandra* observations very well (Rho et al. 2002). The rolloff frequencies found by Rho et al. (2002) were in the range of $(8 - 10) \times 10^{16}$ Hz. Optically observed shocks have speeds of 400–900 km s^{-1}, which could with difficulty produce the observed rolloffs; but broad Fe Kα emission (Ueno et al. 2007) suggests more typical shock velocities closer to 2000 km s^{-1}.

It has been argued that the continuum could still be nonthermal bremsstrahlung, but more recent observations with *XMM-Newton* (Vink et al. 2006) confirm the synchrotron interpretation with coverage of the rest of the remnant. The synchrotron morphology is unlike that of other young remnants; it is dominantly diffuse, and those filaments that are seen are considerably broader than in Tycho, SN 1006, and Cas A. Vink et al. (2006) described the synchrotron emission in the NE with a power-law of photon index $\Gamma = 2.82 \pm 0.04$; the somewhat steep value is consistent with the fairly low rolloff frequencies found in the SW.

6.7. Other Candidates for X-Ray-Synchrotron Domination

Various other objects have been proposed as candidates for X-ray synchrotron radiation. Torii et al. (2006) report ASCA observations showing diffuse X-ray emission with a featureless spectrum (power-law photon index $\Gamma = 2.8 \pm 0.2$) from the interior of a partial radio shell remnant G330.2+1.0 about 11 arcmin in diameter. Bamba et al. (2004) report a nonthermal component in X-ray emission from the superbubble 30 Dor C in the Large Magellanic Cloud. It is a nearly complete X-ray shell; emission from the south is thermal, but that from the N and W is well described by a power-law with $\Gamma = 2.1 - 2.9$, varying somewhat with position. The ASCA Galactic Plane Survey (AGPS) turned up several candidates. One such source is AX J1843.8-0352 (Ueno et al. 2003), associated with the radio SNR G28.6-0.1, with a spectrum that could be fit with a power-law with $\Gamma = 2.1$. *Chandra* observations showed that part of the emission was thermal, but confirmed the nonthermal nature of the rest. Bamba et al. (2003a) reported hard, featureless spectra from three diffuse sources. Two more sources found in the AGPS were followed-up on with *XMM-Newton* (Yamaguchi et al. 2004); one, G32.45+0.1, appears to be a nonthermal shell with $\Gamma = 2.2$, with extremely high absorption. All these cases await further investigation.

A fourth X-ray-synchrotron-dominated shell remnant, G1.9+0.3, has very recently been discovered (Reynolds et al. 2008). It turns out to be the youngest SNR in the Galaxy, with an age of 140 $\pm$ 30 years, or less if deceleration has occurred. Very high obscuration indicates a distance of order that to the Galactic Center (8.5 kpc), at which the shock velocity is about 14,000 km s^{-1}. The roll-off frequency is one of the highest ever reported, $h\nu_{\text{roll-off}} \sim 6$ keV. Only a radio counterpart is known. This object will be the focus of intense study in the near future.

6.8. EGRET Candidates

Esposito et al. (1996) found five candidate associations between EGRET sources and known SNRs. The two strongest, γCyg and IC 443, both had power-law spectra with $\Gamma \sim 2.0$ and integral fluxes above 100 MeV of order 10^{-7} photons cm^{-2} s^{-1}. Both were shown to be explainable by suitable combinations of π^0-decay and bremsstrahlung by Gaisser, Protheroe & Stanev (1998). Neither of these objects shows evidence for significant nonthermal X-rays. In IC 443, the EGRET error circle does not contain any of several hard X-ray knots, or a known PWN (Bocchino & Bykov 2003).

Torres et al. (2003) list and thoroughly review about 20 candidate SNR associations based on positional coincidence with sources from the 3EGC. They also summarize GeV photon production mechanisms, including the propagation and diffusion of relativistic ions away from SNRs and into nearby molecular clouds. The energy distribution of such ions will differ from that behind the shock, both because lower-energy fast ions cannot escape as easily and have a shorter precursor, but also because of diffusive effects once ions have left the neighborhood of the shock. Such effects should produce a steepened ion distribution compared to the postshock one, but with a low-energy cutoff. Torres et al. (2003) also cite seven more shell SNRs near 3EG sources that might emit by this process. Torres et al. (2003) estimate that the chance of all of their candidate associations being chance coincidences is about 10^{-5}; they regard some of their list of coincidences as "promising," though none can be regarded as conclusive at this point. This situation should be greatly improved by the GLAST mission.

6.9. TeV Candidates

IC 443 has a reported 5.7 σ detection with MAGIC (Albert et al. 2007), with a power-law spectral fit $F(E) = (1.0 \pm 0.2) \times 10^{-11}(E/0.4\ \text{TeV})^{-3.1\pm0.3}$ photons cm^{-2} s^{-1} TeV^{-1}. The source is not quite coincident with the EGRET error circle, nor with any of the hard X-ray sources. In addition to observations mentioned above, the HESS collaboration has reported the discovery of 14 low-Galactic-latitude TeV sources without obvious counterparts (Aharonian et al. 2006). Many efforts have been made to identify these; at least one, HESS J1813-178, seems to be associated with a previously unknown shell SNR (Brogan et al. 2005), whereas others may be pulsars or PWN. Follow-up studies continue. The Milagro collaboration has reported several Galactic-plane detections (Abdo et al. 2007), though without clear SNR associations at this time.

7. CONFRONTATION OF OBSERVATIONS AND THEORY

7.1. Magnetic-Field Amplification

Evidence has been mounting for decades that magnetic fields in SNRs can be considerably higher than simple compression would suggest. In Cas A, a lower limit on the magnetic-field strength of 0.8 mG was deduced by Cowsik & Sarkar (1980) from early upper limits on electron bremsstrahlung emission above 100 MeV from COS-B and SAS-2, which bound the relativistic-electron density from above, requiring a minimum magnetic-field strength to produce the observed synchrotron fluxes. The model of Reynolds & Chevalier (1981) required a loss-steepened electron spectrum in SN 1006 and $B \sim 220\ \mu$G. Current TeV upper limits for SN 1006 put limits on ICCMB emission, and require $B \gtrsim 25\ \mu$G (Aharonian et al. 2005). The upper limit for Tycho described above (Aharonian et al. 2001a) required $B \gtrsim 22\ \mu$G if the RXTE spectrum (Allen, Gotthelf & Petre 1999) were due to synchrotron radiation, but if that emission could be explained by, say, bremsstrahlung, the limit dropped to 6 μG. These limits apply to the remnant as a whole. The strongest argument for higher magnetic fields in close proximity to the shock is that synchrotron X-ray emission is often (but not always) in very thin filaments parallel to the remnant edge. The required drop in synchrotron emissivity behind the shock is far too fast to be explained by adiabatic expansion on electrons and magnetic field, so it requires either that X-ray-emitting electrons disappear through radiative losses (e.g., Vink & Laming 2003), or magnetic field disappears through some damping mechanism (Pohl, Yan & Lazarian 2005). If electron losses are the cause, the magnetic field strength is fixed by the filament widths, which are the distance electrons convect in the postshock flow in a synchrotron loss time. Typical filament thicknesses l are of order 0.01 pc, giving (Parizot et al. 2006)

$$B \gtrsim 200\, u_8^{2/3} (l/0.01\ \mathrm{pc})^{-2/3}\ \mu\mathrm{G} \tag{48}$$

and implying immediate postshock magnetic field strengths between 50 μG and 200 μG for the historical SNRs. Unless compression ratios are far larger than expected even with efficient particle acceleration, these values require additional amplification, perhaps through the Bell-Lucek mechanism (Lucek & Bell 2000, Bell & Lucek 2001). However, it is not completely clear whether the required field strength is manifested in steady, nonzero-mean field or is in the form of high-amplitude waves. Thin rims in high-resolution radio images of some remnants (Reynolds 1988b) cannot be due to synchrotron losses and might require wave damping. The question can be addressed observationally, though results so far are ambiguous (Cassam-Chenaï et al. 2007). The observations of X-ray variability in G347.3–0.5 (Uchiyama et al. 2007), if reflective of the actual acceleration and loss timescales, could be explained by either steady or transient amplified magnetic field.

Strong magnetic-field amplification can help solve another puzzle with synchrotron X-ray morphology. X-ray emitting electrons have potentially resolvable diffusion lengths $l_D \sim \kappa/u$ ahead of the shock in the historical shells. Although the magnetic field is lower ahead of the shock, the electron distribution is continuous at the shock and drops at most exponentially with e-folding scale l_D—producing a potentially observable synchrotron halo. For SN 1006, with the sharpest edges and the least thermal contamination, the synchrotron intensity seems to jump by a factor of at least 70 at the shock in the NE (Long et al. 2003), though considerably brighter halo emission was predicted (Reynolds 1998). Although the magnetic-field amplification process described in Lucek & Bell (2000) seems also to require a magnetic precursor on the same diffusion-length scale as fast particles, that scale is much shorter for higher fields, $\kappa \propto B^{-1}$ for constant gyrofactor. If B is sufficiently large, the precursor scale can be smaller than the resolution, so that the halo is very thin and unobservable.

The detailed plasma physics of magnetic-field amplification in shock waves is still under study, but the consequences of strong shocks putting large fractions of shock energy into magnetic field would extend across astrophysics. Just for the question of particle acceleration, the existence of such amplification has been used to argue that shocks must be efficient, hence that accelerated ions must be present in SNRs (e.g., Berezhko, Ksenofontov, & Völk 2003). Although the existence of some kind of amplification does now seem certain, almost all details are still obscure: How does the process depend on shock speed, obliquity, or upstream ionization state? How might it affect, or be affected by, particle injection? Progress on these questions will almost certainly require observations that can detect energetic electrons apart from the magnetic field, such as GLAST observations of nonthermal bremsstrahlung.

7.2. Conclusions from keV, MeV-GeV, and TeV Observations

Radio spectra and images from SNRs have provided important tests and constraints on the theory of particle acceleration. However, one of the strengths of DSA—its prediction of the accelerated particle power-law spectrum almost independent of other parameters—also means that little can be deduced from observing the power-law or near power-law portion of particle spectra. In addition, the presence of fast ions has no direct signature below MeV photon energies. Furthermore, the exclusive reliance on synchrotron radiation as an emission process convolves the observed spectra and morphologies of SNRs with unknown properties of the magnetic field. Many of these problems are ameliorated at keV energies and above. First, synchrotron spectra are cutting off there, so that the physics of the maximum-energy limitation is now accessible (though combined in one parameter, the cutoff energy). Second, suprathermal bremsstrahlung, IC emission, and π^0-decay emission provide more direct information on particle spectra without the necessity of understanding the magnetic field (though requiring other ancillary knowledge, such as of ambient material or radiation fields).

7.2.1. X-rays. The discovery of 100-TeV electrons in SNRs through synchrotron radiation has been an important step forward, but it has not answered all questions about particle acceleration. At the most basic level, we still do not know the efficiency of shock acceleration: the fraction of shock energy winding up in fast electrons and ions. Unless we can determine the efficiency as a function of other shock parameters, it is unlikely that we will come to understand the theoretical problem of electron injection into the DSA process. However, the basic estimates of DSA for maximum energies (Equations 26–28) are consistent with the observations; in most cases it cannot be determined which mechanism is responsible without additional information.

An important result from the X-ray regime is a negative one: No known SNR exhibits an unbroken power-law of synchrotron emission from radio to X-rays (Reynolds & Keohane 1999). That is, for electrons $E_{\max} < 100(B/10\ \mu\mathrm{G})^{1/2}$ TeV. Even for very high magnetic-field strengths of 1 mG, the electron spectra we currently observe in SNRs have begun steepening below the knee energy of about 3000 TeV. If electron acceleration is loss-limited, $E_{\max} \propto B^{-1/2}$ (Equation 27), so the corresponding photon energy $h\nu_{\max} \propto E_{\max}^2 B$ is independent of magnetic-field strength. However, if electron acceleration is loss-limited in all cases, it is possible that ion acceleration can continue to higher energies.

The obliquity dependence of particle injection and acceleration in shocks is still unknown, but susceptible to study with X-ray observations. For a Type Ia remnant expected to be encountering undisturbed ISM, the shock ought to have different obliquities at different points on the perimeter (although sufficiently strong upstream turbulence may render the obliquity time-variable and poorly defined on small scales). Dyer et al. (2001) assumed that in SN 1006, the bright opposing rims are equatorial belts where the shocks are nearly perpendicular, as acceleration rates can be larger there as described above. The ambient magnetic-field direction would then be SE-NW. However, Rothenflug et al. (2004) concluded that the bright rims are polar caps with a presumed ambient magnetic-field direction NE-SW, based on departures of large-scale X-ray morphology from the expectations of an axially symmetric belt model. This question is not settled; SN 1006 clearly has front-to-back asymmetries (Hamilton et al. 1997), but a caps model seen end-on would not resemble any known SNR, so SN 1006 would have to be even more special than it already appears to be. More detailed modeling of the radio structure might be profitable. In either case, the observed variations in rolloff frequency with position seen by Rothenflug et al. (2004) cannot be ascribed to magnetic-field variations and are too large to be shock-velocity variations, so they are presumed to be due to obliquity effects. Obliquity-dependent injection might alter the overall relativistic-particle population, but should not affect the spectral shape addressed by the rolloff frequency. These important data are yet to be modeled adequately. Unfortunately, few other SNRs are suitable for this kind of study.

7.2.2. MeV-GeV observations. We already know from radio observations that SNRs contain particles (electrons) with energies up to about 10 GeV, so the maximum-energy requirements for particles emitting this range of photon energies are evidently easily achieved. With the possible exception of a handful of objects from the EGRET catalogs (Esposito et al. 1996), there are only upper limits here, though these can be valuable in broad-band modeling (see **Figure 5**). So far, those limits do not exclude large classes of models, but can limit available parameter space.

The EGRET sources coincident with SNRs, if actually associated, are relatively unconstraining (see **Figure 4**). It is clear that various combinations of processes could describe these spectra. In principle, more secure detections could allow the inference of the electron distribution, allowing the measurement of the efficiency of electron acceleration, but even if a detection can be firmly attributed to bremsstrahlung, this may be a difficult task. For instance, young remnants typically have heavy-element ejecta mixed close to the outer blast wave; if blast-wave-accelerated electrons diffuse into ejecta clumps, the Z^2 dependence of bremsstrahlung could impede the extraction of the fast-electron spectrum's normalization.

The most tantalizing possibility in this energy range is the unequivocal detection of the π^0 bump around 70 MeV that would signal the direct detection of accelerated ions. This would be a great advance, but it is also possible that bremsstrahlung and IC emission will confuse such emission. Fortunately, the required target population may manifest itself directly, for instance in the form of thermal X-ray emission. Detailed modeling will likely be required in any case.

7.2.3. TeV observations. For none of the detected objects has an airtight case been made in favor of one of the three possible emission processes, though in most cases the only competitors are ICCMB and π^0 decay. In the case of G347.3-0.5, significant problems affect either explanation (Aharonian et al. 2007b). However, any detection produces at least a lower limit on the magnetic-field strength, because it is certainly an upper limit to any ICCMB contribution. (There is some model dependence in this inference, involving quantities such as magnetic-field filling factors.) Models seem able to describe fairly well the detected TeV spectra, even with sometimes troublesome limits at GeV energies. We are not yet ready to use TeV detections to infer detailed source properties or to test shock-acceleration physics in detail. If emission can be shown firmly to be from π^0 decay, we learn the product of the accelerated-particle and thermal target densities, so extracting the former (again, highly desirable as a direct measure of shock-acceleration efficiency) still relies on independent inferences of the thermal-gas density. However, we will certainly be in the part of the spectrum where the ion distribution is cutting off, so once again the physics of E_{max} is accessible.

8. SUMMARY AND FUTURE PROSPECTS

High-energy emission from shell supernova remnants has given us the clearest look at mechanisms for the production of high-energy nonthermal particle distributions, mechanisms that might well operate in a wide range of astrophysical environments. The presence of 100-TeV electrons in several shell remnants is now established; theoretical models seem quite able to describe the observations with diffusive shock acceleration theory, coupled to SNR evolution. However, observations cannot yet be used to constrain models in detail. Although cosmic-ray ions have not yet been directly detected, many indirect lines of evidence point to efficient shock acceleration, which requires the presence of energetic ions.

The excitement of the detection of nonthermal X-ray and gamma-ray emission from SNRs should not blind us to the substantial unfinished business ahead. We still have no universally agreed-on mechanism for electron injection. We cannot predict from first principles the efficiency of acceleration of either electrons or ions. We do not know the detailed physics of magnetic-field amplification, or how it depends on shock speed, upstream ionized fraction or other parameters. We have no idea how any of these depends on shock obliquity. Finally, we do not seem to need to invoke particle acceleration at reverse shocks, except in rare cases (Rho et al. 2002), but we don't know why not. The magnetic field might be weak; why then don't reverse shocks amplify magnetic field?

Immediate progress should be possible with GLAST. Its peak sensitivity is about two orders-of-magnitude better than EGRET; though at 70 MeV, where the important π^0 bump is expected, the effective area is only about 25% of its maximum, which is attained between about 2 and 200 GeV. It should still allow detection of GeV bremsstrahlung from substantial numbers of SNRs, but even nondetections are important, as they provide lower limits on magnetic field and may therefore add evidence for amplification of magnetic field over large volumes, not just the thin rims occupied by synchrotron X-rays. Another promising avenue for observational progress is increased sensitivity of ground-based air-Čerenkov telescopes, gained primarily by lowering the minimum threshold energy at which air showers can be detected; because almost all spectra are steeply falling at TeV energies, a relatively small decrease in that threshold can provide substantial increases in sensitivity. Finally, interesting targets remain to be discovered; the newest synchrotron-dominated X-ray SNR, G1.9+0.3, is an example.

Particle acceleration to high energies can now be addressed by fairly direct investigation. We should not neglect the untapped potential of radio observations for understanding electron injection, acceleration, and propagation. New types of constraints may emerge from new areas, such as X-ray polarimetry. Our search for the understanding of SNR observations, and for the origin of cosmic rays, has produced unexpected byproducts such as evidence for strong magnetic-field amplification. GLAST and other near-future missions should provide exciting advances over the next few years; theoretical work must move beyond simply finding models that can explain what is seen, and begin making discriminations.

DISCLOSURE STATEMENT

The author is not aware of any biases that might be perceived as affecting the objectivity of this review.

ACKNOWLEDGMENTS

I would like to thank John Blondin, Kazik Borkowski, Roger Chevalier, Don Ellison, Una Hwang, and Pat Slane for helpful comments on the manuscript. I am grateful to NASA for ongoing support through Astrophysics Theory Program grants and various observing programs.

LITERATURE CITED

Abdo AA, Allen B, Berley D, Casanova S, Chen C, et al. 2007. *Ap. J.* 664:L91
Achterberg A, Blandford RD, Reynolds SP. 1994. *Astron. Astrophys.* 281:220
Aharonian F, Akhperjanian A, Barrio J, Bernlöhr K, Börst H, et al. 2001a. *Astron. Astrophys.* 370:112

Aharonian F, Akhperjanian AG, Aye K-M, Bazer-Bachi AR, Beilicke M, et al. 2005. *Astron. Astrophys.* 437:135
Aharonian F, Akhperjanian AG, Bazer-Bachi AR, Beilicke M, Benbow W, et al. 2006. *Ap. J.* 636:777
Aharonian F, Akhperjanian AG, Bazer-Bachi AR, Beilicke M, Benbow W, et al. 2007a. *Ap. J.* 661:236
Aharonian F, Akhperjanian AG, Bazer-Bachi AR, Beilicke M, Benbow W, et al. 2007b. *Astron. Astrophys.* 464:235
Aharonian FA, Akhperjanian AG, Barrio J, Bernlöhr K, Börst H, et al. 2001b. *Astron. Astrophys.* 373:292
Aharonian FA, Atoyan AM. 1999. *Astron. Astrophys.* 351:330
Albert J, Aliu E, Anderhub H, Antoranz P, Armada A, et al. 2007. *Ap. J. Lett.* 664:L87
Allen GE, Gotthelf EV, Petre R. 1999. *Proc. 26th Int. Cosmic Ray Conf.* 3:480
Allen GE, Keohane JW, Gotthelf EV, Petre R, Jahoda K, et al. 1997. *Ap. J. Lett.* 487:L97
Amato E, Blasi P. 2006. *MNRAS* 371:1251
Ammosov AE, Ksenofontov LT, Nikolaev VS, Petukhov SI. 1994. *Astron. Lett.* 20:157
Aschenbach B. 1998. *Nature* 396:141
Axford WI, Leer E, Skadron G. 1977. *Proc.15th Int.Cosmic Ray Conf.* 11:132
Bamba A, Ueno M, Koyama K, Yamauchi S. 2003a. *Ap. J.* 589:253
Bamba A, Ueno M, Nakajima H, Koyama K. 2004. *Ap. J.* 602:257
Bamba A, Yamazaki R, Hiraga JS. 2005. *Ap. J.* 632:294
Bamba A, Yamazaki R, Ueno M, Koyama K. 2003b. *Ap. J.* 589:827
Bamba A, Yamazaki R, Yoshida T, Terasawa T, Koyama K. 2005. *Ap. J.* 621:793
Baring MG, Ellison DC, Reynolds SP, Grenier IA, Goret P. 1999. *Ap. J.* 513:311
Becker RH, Szymkowiak AE, Boldt EA, Holt SS, Serlemitsos PJ. 1980. *Ap. J. Lett.* 240:L33
Bell AR. 1978. *MNRAS* 182:147
Bell AR. 1987. *MNRAS* 225:615
Bell AR, Lucek SG. 2001. *MNRAS* 321:433
Berezhko EG. 1996. *Astropart. Phys.* 5:367
Berezhko EG, Ellison DC. 1999. *Ap. J.* 526:385
Berezhko EG, Elshin VK, Ksenofontov LT. 1996. *JETP* 82:1
Berezhko EG, Ksenofontov LT, Völk H. 2003. *Astron. Astrophys.* 412:L11
Berezhko EG, Völk H. 2006. *Astron. Astrophys.* 451:981
Blandford RD, Cowie LL. 1982. *Ap. J.* 260:625
Blandford RD, Eichler D. 1987. *Phys. Rep.* 154:1
Blandford RD, Funk. 2007. In *First GLAST Symp.*, ed. S Ritz, P Michelson, C Meegan, p. 62. New York: Am. Inst. Phys.
Blandford RD, Ostriker JP. 1978. *Ap. J. Lett.* 221:L29
Bleeker JAM, Willingale R, van der Heyden K, Dennerl K, Kaastra JS, et al. 2001. *Astron. Astrophys.* 365:L225
Blondin JM, Wright EB, Borkowski KJ, Reynolds SP. 1998. *Ap. J.* 500:342
Bocchino F, Bykov AM. 2003. *Astron. Astrophys.* 400:203
Brogan CL, Gaensler BM, Gelfand JD, Lazendić JS, Lazio TJW, et al. 2005. *Ap. J. Lett.* 629:L105
Butt YM, Torres DF, Combi JA, Dame T, Romero GE. 2001. *Ap. J. Lett.* 562:L167
Cassam-Chenaï G, Decourchelle A, Ballet J, Hwang U, Hughes JP, Petre R. 2004a. *Astron. Astrophys.* 414:545
Cassam-Chenaï G, Decourchelle A, Ballet J, Sauvageot J-L, Dubner G, Giacani E. 2004b. *Astron. Astrophys.* 427:199
Cassam-Chenaï G, Hughes JP, Ballet J, Decourchelle A. 2007. *Ap. J.* 665:315
Chevalier RA. 1977. *Nature* 266:701
Chevalier RA. 1982. *Ap. J.* 258:790
Colgate SA, McKee C. 1969. *Ap. J.* 157:623
Combi JA, Romero GE, Benaglia P. 1999. *Ap. J. Lett.* 519:L177
Cowsik R, Sarkar S. 1980. *MNRAS* 191:855
Dermer CD. 1986a. *Ap. J.* 307:47
Dermer CD. 1986b. *Astron. Astrophys.* 157:223
Drury LO'C. 1983. *Rep. Progr. Phys.* 46:973

Drury LO'C. 1991. *MNRAS* 251:340
Drury LO'C, Aharonian FA, Völk HJ. 1994. *Astron. Astrophys.* 287:959
Drury LO'C, Duffy P, Kirk JG. 1996. *Astron. Astrophys.* 309:1002
Drury LO'C, Völk HJ. 1981. *Ap. J.* 248:344
Duncan AR, Green DA. 2000. *Astron. Astrophys.* 364:732
Dwarkadas VV, Chevalier RA. 1998. *Ap. J.* 497:807
Dyer KK, Reynolds SP, Borkowski KJ, Allen GE, Petre R. 2001. *Ap. J.* 551:439
Eichler D. 1979. *Ap. J.* 229:419
Eichler D. 1984. *Ap. J.* 277:429
Ellison DC, Baring MG, Jones FC. 1995. *Ap. J.* 453:873
Ellison DC, Berezhko EG, Baring MG. 2000. *Ap. J.* 540:292
Ellison DC, Cassam-Chenaï G. 2005. *Ap. J.* 632:920
Ellison DC, Decourchelle A, Ballet J. 2004. *Astron. Astrophys.* 413:189
Ellison DC, Eichler D. 1984. *Ap. J.* 286:691
Ellison DC, Reynolds SP. 1991. *Ap. J.* 382:242
Enomoto R, Tanimori T, Naito T, Yoshida T, Yanagita S, et al. 2002. *Nature* 416:823
Esposito JA, Hunter SD, Kanbach G, Sreekumar P. 1996. *Ap. J.* 461:820
Falle SAEG, Giddings JR. 1987. *MNRAS* 225:399
Favata F, Vink J, dal Fiume D, Parmar AN, Santangelo A, et al. 1997. *Astron. Astrophys.* 324:L49
Fermi E. 1949. *Phys. Rev.* 75:1169
Gaisser TK. 1990. *Cosmic Rays and Particle Physics*. Cambridge, UK: Cambridge Univ. Press
Gaisser TK, Protheroe RJ, Stanev T. 1998. *Ap. J.* 492:219
Galas CMF, Venkatesan D, Garmire G. 1982. *Ap. Lett.* 22:103
Giacalone J, Jokipii JR. 1994. *Ap. J. Lett.* 430:L137
Gotthelf EV, Koralesky B, Rudnick L, Jones TW, Hwang U, Petre R. 2001. *Ap. J. Lett.* 552:L39
Green DA. 2006. *A Catalogue of Galactic Supernova Remnants* (2006 April version), Astrophys. Group, Cavendish Lab., Cambridge, UK (URL: **http://www.mrao.cam.ac.uk/surveys/snrs/**)
Hamilton AJS, Fesen RA, Wu C-C, Crenshaw DM, Sarazin CL. 1997. *Ap. J.* 481:838
Hartman RC, Bertsch DL, Bloom SD, Chen AW, Deines-Jones P, et al. 1999. *Ap. J. Suppl.* 123:79
Hiraga JS, Uchiyama Y, Takahashi T, Aharonian FA. 2005. *Astron. Astrophys.* 431:953
Houck JC, Allen GE. 2006. *Ap. J. Suppl.* 167:26
Hwang U, Decourchelle A, Holt SS, Petre R. 2002. *Ap. J.* 581:1101
Iyudin AF, Aschenbach B, Becker W, Dennerl K, Haberl F. 2005. *Astron. Astrophys.* 429:225
Iyudin AF, Schönfelder V, Bennett K, Bloemen H, Diehl R, et al. 1998. *Nature* 396:142
Jokipii JR. 1987. *Ap. J.* 313:842
Jones FC. 1968. *Phys. Rev.* 167:1159
Jones FC, Ellison DC. 1991. *Space Sci. Rev.* 58:259
Kalemci E, Reynolds SP, Boggs SE, Lund N, Chenevez J, et al. 2006. *Ap. J.* 644:274
Kang H, Jones TW. 1995. *Ap. J.* 447:944
Katagiri H, Enomoto R, Ksenofontov LT, Mori M, Adachi Y, et al. 2005. *Ap. J. Lett.* 619:L163
Koyama K, Kinugasa K, Matsuzaki K, Nishiuchi M, Sugizaki M, et al. 1997. *Publ. Astron. Soc. Jpn.* 49:L7
Koyama K, Petre R, Gotthelf EV, Hwang U, Matsuura M, et al. 1995. *Nature* 378:255
Krymsky GF. 1977. *Sov. Phys. Dokl.* 22:327
Ksenofontov LT, Berezhko EG, Völk HJ. 2005. *Astron. Astrophys.* 443:973
Lagage PO, Cesarsky CJ. 1983. *Astron. Astrophys.* 125:249
Laming JM. 1998. *Ap. J.* 499:309
Lazendić JS, Slane PO, Gaensler BM, Reynolds SP, Plucinsky PP, Hughes JP. 2004. *Ap. J.* 602:271
Long KS, Reynolds SP, Raymond JC, Winkler PF, Dyer KK, Petre R. 2003. *Ap. J.* 586:1162
Lucek SG, Bell AR. 2000. *MNRAS* 314:65
Malkov MA, Drury LO'C. 2001. *Rep. Progr. Phys.* 64:429
Mastichiadis A. 1996. *Astron. Astrophys.* 305:L53
Matzner CD, McKee CF. 1999. *Ap. J.* 510:379
Melrose DB. 1974. *Sol. Phys.* 37:353

Minnie J, Bieber JW, Matthaeus WH, Burger RA. 2007. *Ap. J.* 663:1049
Moffett DA, Goss WM, Reynolds SP. 1993. *Astron. J.* 106:1566
Nadyozhin DK. 1985. *Astrophys. Space Sci.* 112:225
Naito T, Takahara F. 1994. *J. Phys. G: Nuclear Part. Phys.* 20:477
Ostrowski M. 1999. *Astron. Astrophys.* 345:256
Pacholczyk AG. 1970. *Radio Astrophysics: Non-Thermal Processes in Galactic and Extragalactic Sources.* San Francisco: Freeman
Parizot E, Marcowith A, Ballet J, Gallant YA. 2006. *Astron. Astrophys.* 453:387
Pavlov GG, Sanwal D, Kiziltan B, Garmire GP. 2001. *Ap. J. Lett.* 559:L131
Pohl M. 1996. *Astron. Astrophys.* 307:L57
Pohl M, Yan H, Lazarian A. 2005. *Ap. J. Lett.* 626:L101
Quest K. 1988. *J. Geophys. Res.* 93:9649
Reynolds SP. 1988a. In *Galactic and Extragalactic Radio Astronomy*, ed. KI Kellermann, GL Verschuur, p. 439. Berlin: Springer
Reynolds SP. 1988b. In *Supernova Remnants and the Interstellar Medium*, ed. RS Roger, TL Landecker, p. 331. Cambridge, UK: Cambridge Univ. Press
Reynolds SP. 1998. *Ap. J.* 493:375
Reynolds SP, Borkowski KJ, Green DA, Hwang U, Harrus I, Petre R. 2008. *Ap. J.* 680:L41 *Erratum
Reynolds SP, Chevalier RA. 1981. *Ap. J.* 245:912
Reynolds SP, Keohane JW. 1999. *Ap. J.* 525:368
Rho J, Dyer KK, Borkowski KJ, Reynolds SP. 2002. *Ap. J.* 581:1116
Roberts MSE, Tam CR, Kaspi VM, Lyutikov M, Vasisht G, et al. 2003. *Ap. J.* 588:992
Rothenflug R, Ballet J, Dubner G, Giacani E, Decourchelle A, Ferrando P. 2004. *Astron. Astrophys.* 425:121
Schönfelder V, Bloemen H, Collmar W, Diehl R, Hermsen W, et al. 2000. In *Proc. Fifth Compton Symp.*, ed. ML McConnell, JM Ryan, p. 54. New York: Am. Inst. Phys.
Sedov LI. 1959. *Similarity and Dimensional Methods in Mechanics*. New York: Academic
Shklovskii IS. 1953. *Dokl. Akad. Nauk. SSSR* 91:475
Sinitsyna VG, Arsov TP, Borisov SS, Musin FI, Nikolsky SI, et al. 2005. In *Proc. 29th Int. Cosmic Ray Conf.* 4:231
Slane P, Gaensler BM, Dame TM, Hughes JP, Plucinsky PP, Green A. 1999. *Ap. J.* 525:357
Slane PO, Hughes JP, Edgar RJ, Plucinsky PP, Miyata E, et al. 2001. *Ap. J.* 548:814
Spitzer L. 1978. *Physical Processes in the Interstellar Medium*. New York: Wiley
Sturner SJ, Skibo JG, Dermer CD, Mattox JR. 1997. *Ap. J.* 490:619
The L-S, Leising MD, Kurfess JD, Johnson WN, Hartmann DH, et al. 1996. *Astron. Astrophys. Suppl.* 120:357
Torii K, Uchida H, Hasuike K, Tsunemi H, Yamaguchi Y, Shibata S. 2006. *Publ. Astron. Soc. Jpn.* 58:L11
Torres DF, Romero GE, Dame TM, Combi JA, Butt YM. 2003. *Phys. Rep.* 382:303
Truelove JK, McKee CF. 1999. *Ap. J. Suppl.* 120:299
Tsunemi H, Miyata E, Aschenbach B, Hiraga J, Akutsu D. 2000. *Publ. Astron. Soc. Jpn.* 52:887
Uchiyama Y, Aharonian FA, Takahashi T. 2003. *Astron. Astrophys.* 400:567
Uchiyama Y, Aharonian FA, Tanaka T, Takahashi T, Maeda Y. 2007. *Nature* 449:576
Ueno M, Bamba A, Koyama K, Ebisawa K. 2003. *Ap. J.* 588:338
Ueno M, Sato R, Kataoka J, Bamba A, Harrus I, et al. 2007. *Publ. Astron. Soc. Jpn.* 59:S171
Vink J, Bleeker J, van der Heyden K, Bykov A, Bamba A, Yamazaki R. 2006. *Ap. J. Lett.* 648:L33
Vink J, Laming JM. 2003. *Ap. J.* 584:758
Vladimirov A, Ellison DC, Bykov A. 2006. *Ap. J.* 652:1246
Völk HJ, Berezhko EG, Ksenofontov LT. 2007. *Astrophys. Space Sci.* 309:389
Warren JS, Hughes JP, Badenes C, Ghavamian P, McKee CF, et al. 2005. *Ap. J.* 634:376
Webb GM, Drury LO'C, Biermann PL. 1984. *Astron. Astrophys.* 137:185
Yamaguchi H, Ueno M, Koyama K, Bamba A, Yamauchi S. 2004. *Publ. Astron. Soc. Jpn.* 56:1059
Yamazaki R, Kohri K, Bamba A, Yoshida T, Tsuribe T, Takahara F. 2006. *MNRAS* 371:1975

RELATED RESOURCES

Blumenthal GR, Gould RJ. 1970. Bremsstrahlung, synchrotron radiation, and Compton scattering of high-energy electrons traversing dilute gases. *Rev. Mod. Phys.* 42:237

Draine BT, McKee CF. 1993. Theory of interstellar shocks. *Annu. Rev. Astron. Astrophys.* 31:373

Ostriker JP, McKee CF. 1988. Astrophysical blastwaves. *Rev. Mod. Phys.* 60:1

Trimble V. 1982. Supernovae. Part I: the events. *Rev. Mod. Phys.* 54:1183

Trimble V. 1983. Supernovae. Part II: the aftermath. *Rev. Mod. Phys.* 55:511

Annual Review of
Astronomy and
Astrophysics

Volume 46, 2008

Contents

Indexes

Errata

An online log of corrections to *Annual Review of Astronomy and Astrophysics* articles may be found at http://astro.annualreviews.org/errata.shtml